Influence of mixed-frequency medium-voltage and environmental stress on the aging of epoxy

Journal Article

Author(s):
Küchler, Florian (iD); Färber, Raphael (iD); Sefl, Ondrej (iD); Bill, Fabian; Franck, Christian (iD)

Influence of mixed-frequency medium-voltage and environmental stress on the aging of epoxy

Florian Küchler[*]👤, **Raphael Färber, Ondřej Šefl, Fabian Bill and Christian M Franck**👤

High Voltage Laboratory, ETH Zurich, 8092 Zurich, Switzerland

E-mail: kuechler@eeh.ee.ethz.ch

CrossMark

Abstract

Recent developments in power electronic technologies lead to new challenges for insulation systems. This contribution aims to clarify the influence of a broad range of mixed-frequency (MF) medium-voltage and environmental stress parameters on the aging of epoxy insulation. For this purpose, test samples are stressed with an AC (50 Hz) or a DC voltage, superimposed with a pulse-width-modulated (PWM) voltage (kHz range). An analysis of the samples' health state is carried out after the aging by the evaluation of potential aging markers (AC breakdown strength, dielectric permittivity, glass transition temperature, Fourier-transform infrared spectroscopy spectra). Although the main focus of this work is on aging below the inception of partial discharges (PDs), it was first confirmed that PD-related aging depends mainly on the peak voltage stress. In contrast, the results obtained by aging below PD inception suggests a dependence on the root-mean-square of the applied voltage stress, and consequently on the energy dissipation. Aging in the PD-free regime was only observed at alternating electric field stress and high relative humidity or elevated temperatures. No influences of space charge and of the slew rate of the PWM voltage were observed. Remarkably, higher PWM frequencies lead to less insulation aging. This might be attributed to the increasing hindrance of polymer side chain movement at higher frequencies, as observed by dielectric spectroscopy. In addition, it is indicated that the aging mechanisms under MF voltage stress result from superimposed single-frequency aging mechanisms and that aging is activated after a latency period. Of the investigated potential aging markers, only the residual breakdown strength revealed aging effects, which correlates with lifetime observations in the PD-free voltage stress regime. It is hypothesized that the aging mechanism is associated with a rearrangement of the free volume in the polymer, followed by a localized breaking of van der Waals bonds.

Keywords: insulation aging, inverter voltage stress, epoxy insulation, partial discharge, hygroelectrical stress

(Some figures may appear in colour only in the online journal)

---

[*] Author to whom any correspondence should be addressed.

J. Phys. D: Appl. Phys. **56** (2023) 354005

F Küchler *et al*

1. Introduction

Power electronic components play a vital role in the integration of renewable energy sources in modern energy transmission systems [1–3] as well as in areas with space or weight limitations, such as traction [4] and electric aircraft [5, 6]. The recent progress in wide bandgap semiconductor technologies (SiC and GaN) led to the reduction in power electronics' switching losses thanks to the increased switching speeds ($>10\,kV\,\mu s^{-1}$) [7, 8]. As a result, higher switching frequencies ($>10\,kHz$) [9] can be employed, resulting in higher conversion power densities. Furthermore, higher blocking voltages of SiC- and GaN-based devices ($>2\,kV$) [10–12] pave the way for a growing number of medium-voltage (MV) and high-voltage (HV) applications, e.g. solid-state transformers [4] and inverter-fed MV rotating machines [13]. In general, the trend goes towards higher voltage levels as can be seen by the recent step from 400 V to 800 V systems for electric vehicles [14, 15].

These advancements, however, lead to new challenges for the involved insulation systems, which need to withstand novel types of stresses, such as higher switching speeds (possibly leading to transient overvoltages), higher frequencies and higher voltage levels. Furthermore, voltage waveforms might consist of components with different frequencies, such as sinusoidal 50 Hz voltages with higher-frequency harmonics. As reviewed in an earlier work [16], three main aging regimes are identified in this context.

It was found that partial discharges (PDs) erode the insulation material over time [17–19], depending on the repetition frequency of the PD events, which mainly occur during the pulse slope [19–24]. An increase in the PD amplitudes with increasing slew rate is reported in [21, 25]. It is furthermore noticeable that the partial discharge inception voltage (PDIV) in some cases might be exceeded unexpectedly, e.g. if systemic overvoltages at cable terminations occur [26]. Another example is the decrease in the PDIV at low pressures, which poses a problem in aircraft applications [27]. Moreover, the PDIV was found to be reduced for an increase in the ambient temperature [19, 28], which correlates with reduced lifetime of polymeric materials subjected to PD activity at elevated temperatures [28].

The influence of humidity on the PD behavior is not straightforward. On the one hand, an increasing relative humidity (RH) was found by several authors to decrease the PD activity [29–31] and to increase the insulation lifetime [32–34]. This was mainly attributed to a spreading of PDs over a larger area due to the increased surface conductivity, thus leading to less impact on concentrated locations [33]. On the other hand, also a decrease in lifetime with increasing RH is reported, which, in some cases was only observed above a critical threshold RH_c [32–35]. The lifetime reduction is ascribed either to a removal of surface charge, which should allegedly reduce the number of discharges and average charge, hence reducing the intensity of the aging [32], or to more severe chemical reactions (generating chemical by-products, such as ozone and nitric acids) in

the presence of high RH [36, 37]. Furthermore, the insulation lifetime might decrease for increasing RH even if the PD amplitude decreases [38].

In the absence of PDs, insulation failure might occur due to excessive insulation heating caused by dielectric losses, which are generated during high-frequency switching [17, 23, 39–41]. This might either lead to a thermal breakdown if the heat is not dissipated effectively enough [42, 43] or to enhanced thermally activated aging processes [24, 44].

If neither PD-related aging, nor dielectric heating were present in polymeric insulation, aging was observed empirically [28, 45–47], but the underlying mechanisms were not investigated in detail. In principle, aging in the absence of PDs and dielectric heating can also occur by electromechanical processes, for which different models were developed [48–51]. These models are based on Griffith's theory of fracture mechanics [52] and describe microscopic morphological material changes, such as the formation and growth of microcracks in the (sub-)μm range. These are caused by the electromechanically induced energy dissipation, especially favored to occur in amorphous regions [53, 54]. The morphological changes are attributed to a rearrangement of the free volume (present in the amorphous phase), leading to a deformation/breaking of intermolecular van der Waals bonds with relatively low-energy barriers (compared to those of intramolecular covalent bonds) that have to be exceeded for an onset of aging [50, 54, 55]. These potential energy barriers can be furthermore lowered by an applied electric field and space charges [49, 54], whereas the broken bonds as well as possibly created free radicals are favorable to react with charges and dipoles, such as water [54–56]. If a crack has grown big enough for PD inception to occur, the aging regime shifts to PD erosion. Consequently, electromechanical stress can be regarded as the initiator for fatal aging.

In the case of alternating electric field stress, polymer chains will occupy conformational states that are different from their equilibrium under constant stress. This, in turn, increases the free volume and thus accelerates the formation of voids in amorphous regions. This cyclic stress causes mechanical energy dissipation, which is proportional to the excitation frequency and the fourth power of the electric field [55]. As the electromechanical aging processes are thermally activated, higher temperatures will enhance aging in this regime [49, 51, 54]. In addition, the presence of water is reported to lower the activation energy for bond breaking and the highly polar water molecules might accelerate fatigue processes during applied alternating electric field stress [54]. Mechanical cracking under the influence of combined electric field stress and water is described in [55, 57]. If (sub-)microcracks are filled with a (semi-)conductive medium, such as water, a (field-assisted) crack propagation might occur [48, 58]. Furthermore, water-treeing is reported to appear after stress-cracking [51, 59] and to be faster for increasing frequency [57, 60].

As conclusive knowledge about insulation aging under inverter-type stress in the absence of PDs and dielectric heating is still missing, the goal of this contribution is to clarify

its influence on insulation performance. For this purpose, a systematic study with a focus on a broad range of potential stress parameters is carried out in this work. More specifically, the influence of root-mean-square (RMS) voltage, peak voltage, polarity of voltage, different types of mixed-frequency (MF) voltages, slew rate, frequency and aging time is studied. Additional environmental stress impact is taken into account by aging at different temperatures and humidities (i.e. the water content inside the polymer). In order to show the differences in the aging behavior between the PD-free and the PD-related aging regime, aging tests under PDs are also performed. The health state of samples is evaluated for both PD-free and PD-related aging before and after each aging sequence by means of analysis of potential aging markers, namely short-term AC breakdown strength, complex relative permittivity (real and imaginary parts), volume resistivity, glass transition temperature as well as the chemical composition obtained by Fourier-transform infrared spectroscopy (FTIR).

The aging study in the absence as well as in the presence of PDs follows, in principle, the approach described in a former work [16]. As epoxy is a typical insulation material for inverter-fed rotating machines, an anhydride-cured epoxy is chosen as a sample material and suitable samples were manufactured for PD-free as well as for PD-related aging (section 2.1). Both PD-free and PD aging of these samples is carried out in a suitable temperature/humidity-controlled test bench (section 2.2) which is able to generate a broad range of inverter-type stress profiles (section 2.4). In addition, the PDIV is measured to evaluate the PD aging regime (section 2.3). The analysis of the samples' health state is carried out by measuring the aforementioned potential aging markers. This demands different diagnostic tools, for which either commercial devices or in-house-built devices are used (section 2.5).

2. Methods

In the following section, the sample manufacturing, preparation and conditioning is briefly explained. Subsequently, the used mixed-frequency medium-voltage (MF-MV) aging setup, the measurement principle as well as the aging evaluation approach is described.

2.1. Sample manufacturing, preparation and conditioning

All samples used throughout this work were manufactured from a three-component anhydride-cured epoxy system, consisting mainly of a 2,2-Bis(4-glycidyloxyphenyl)propane resin, a tetrahydro-4-methylphthalic anhydride hardener and a benzyldimethylamine catalyst. The manufacturing steps from the raw materials, provided by Elantas, to the final samples are described in detail in a former work [16].

For PD-free aging, the sample shape was chosen to be recessed, i.e. with a thinner measuring volume of $(200 \pm 10)\,\mu$m thickness (measured for each sample) and a thicker part for mechanical support at the circumference. Pictures of the samples with dimensions are shown in figure 1 (left). The recessed part of the sample was designed with a diameter of 5 mm (the flat part) and the rounding radius of 5 mm (the edge). Silver-coating (SCP Electrolube) of both sides ensured a uniform electric field stress as well as the absence of PDs at the inner part, see figure 1 (right). Aging with PDs was carried out with the same samples, but without silver coating, which favored the inception of PDs near the contacting spherical electrode with a radius of 5 mm, see figure 1 (middle). Both plate and spherical electrodes were made of stainless steel and polished after each aging sequence to eliminate possible protrusions at the electrode surface.

Before conditioning, samples are dried at 50 °C for >24 h according to ISO 62:2008 [61]. It was found by gravimetric analysis (not shown here) that the silver conductive paint is permeable to water. The saturation time of water absorption in the used 200 μm thick samples is estimated as 6.5 h, based on measurements of the diffusion coefficient of the material in thicker, plane samples. Explanations regarding the corresponding measurement and calculation principles can be found in [61, 62]. Thus, conditioning of samples in the desired atmosphere for >24 h is sufficient for saturated (steady-state) water absorption.

In addition to the standard thickness of 200 μm, epoxy samples with thicknesses of 100 μm, 300 μm and 400 μm were manufactured in the same way as described before, in order to investigate the volume/thickness dependence of the short-term AC breakdown strength, see section 2.5.

2.2. MF-MV and ambient stress setup

In order to synthesize inverter-type voltage waveforms for the electrical stressing of the samples, a low-frequency (50 Hz) sinusoidal AC voltage (or a DC voltage) and a pulse-width-modulated (PWM) voltage with high repetition frequency are superimposed, which consequently leads to different MF-MV stress waveforms. Both PD-free or PD-related aging of up to eight samples, connected in parallel, was carried out simultaneously with the setup shown in figure 2. The bipolar PWM voltage is generated with a half-bridge circuit and the coupling capacitor C_2, whereas the rise time of the rectangular pulses can be varied by changing the resistor R_2. The sinusoidal AC voltage was then superimposed at the device-under-test (DUT), which is represented by the eight parallel-connected epoxy samples inside a temperature-controlled test cell. If a DC voltage (of positive polarity) instead of an AC voltage is used, V_{AC} is rectified with a simple rectifier circuit, consisting of a diode and a capacitor, before being superimposed to the PWM voltage. Adjustment of the RH inside the test cell was realized by controlling the flow rate of a dry and humid air flow, which is mixed before entering the test cell. Details of the MF-MV aging setup are described in a former work [16] and the specifications are listed in table 1. Potential effects of ozone, which is generated during PD activity and which might additionally influence the aging behavior [33], were excluded by the constant, humidity-controlled air flow through the test cell.
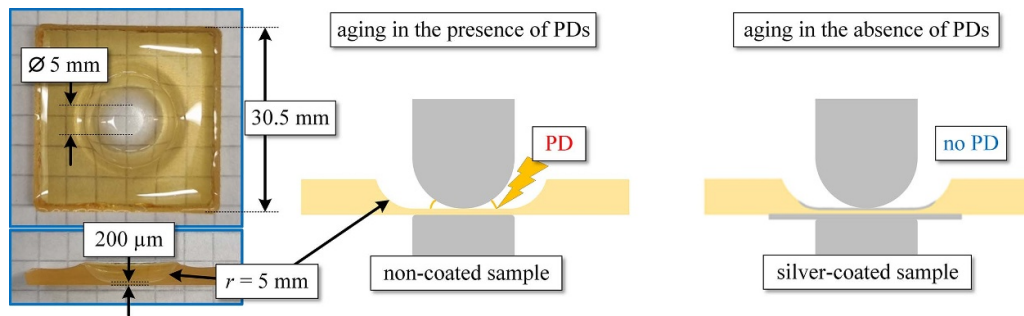
Figure 1. Top view and cross-section of manufactured recessed epoxy samples (left) with schematics of sample-electrode configurations used for aging in the presence (middle) and in the absence (right) of PDs.
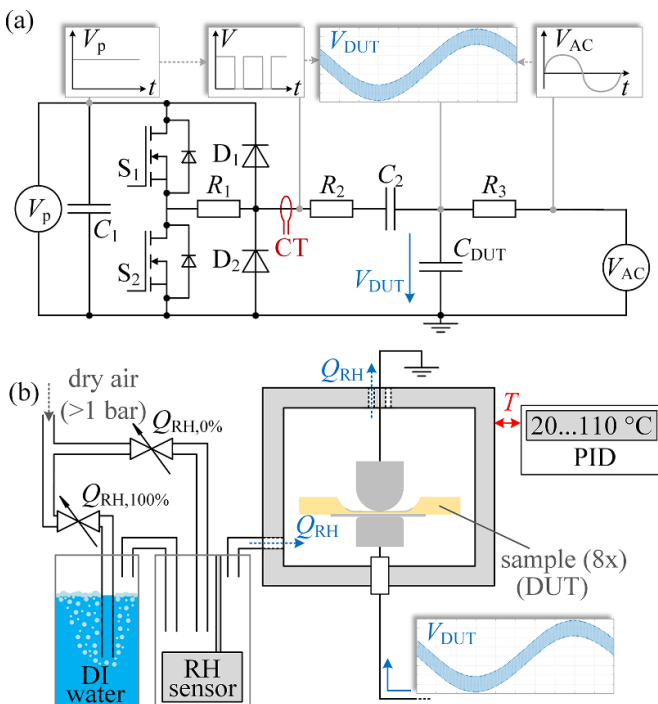

Figure 2. Schematic of mixed-frequency medium-voltage (MF-MV) stress setup (a) and test cell with temperature and humidity control circuits (b).

Table 1. Specifications of the MF-MV and ambient stress setup.

Parameter	Value and unit
AC (50 Hz, RMS) voltage	$0\ldots20$ kV
DC voltage	$0\ldots28$ kV (positive polarity)
PWM voltage	$0\ldots3.5$ kV and $0.1\ldots50$ kHz
Temperature	$20\,°C\ldots110\,°C$
Relative Humidity	$0\%\ldots80\%\pm3\%$ at $22\,°C\pm1\,°C$

2.3. Measurement of the PDIV and characterization of the PD activity

The PDIV of the non-coated epoxy samples was measured to find suitable test voltage levels for subsequent PD aging experiments. Since the test voltage also contains frequency components much larger than 50 Hz, the PDs need to be measured using an alternative (to IEC 60270 [63]) PD instrument. The

instrument of choice is a capacitor connected in series between the test sample and the ground. With suitable decoupling and high enough capacitance, the energy of each PD is deposited practically exclusively into the capacitor, which manifests as an abrupt change of the voltage on its terminals that is linearly proportional to the PD magnitude. Thanks to their very fast fronts, the voltage jumps are readily discernible from the fraction of the test voltage also present on the capacitor terminals (capacitive divider with the test sample). Further description of the method, which is based on the IEC 61934 [64] standard, and the used setup is given in [65].

The PDIV was measured at three frequencies, 50, 1000 and 10 000 Hz, for each condition type (RH = 0% and 75%) to investigate the behavior within the frequency range delimited by the fundamental and pulse repetition frequencies used during aging experiments. As the PDIV measurement setup is not capable of generating PWM voltage waveforms, a sinusoidal test voltage was employed instead. At the beginning of the measurement, the PDIV was roughly estimated by a quick ramp-up of the test voltage. Then, the voltage was reduced to a value at least 200 V(peak) below the level at which no more discharges were detectable, and subsequently gradually increased in steps of about 20 V(peak) every 5 s until the discharge activity was incepted and the PDIV hence determined.

Afterwards, phase-resolved partial discharge (PRPD) patterns at the envisaged aging test voltage of 7.5 kV(peak) were constructed to both characterize the PD activity and provide a tool to quantitatively compare the individual activities under the two condition types (dry vs. humid). The PD activity was always gathered over 1 s from 10 MSa at a sampling frequency of 10 MHz. The magnitude of the discharges was obtained by differentiating the filtered voltage signal of the series capacitor, whereas the zero crossings were determined from the test voltage signal (measured by a HV probe).

2.4. MF-MV and ambient stress

Eight epoxy samples were aged simultaneously in the setup shown in figure 2 with the electrode configurations for either PD-free or PD-related aging described in figure 1. The standard aging conditions subdivided by the main aging regimes are listed in table 2. Note that for different measurements, voltage and ambient stress parameters were changed selectively (usually only one parameter per measurement series) from the
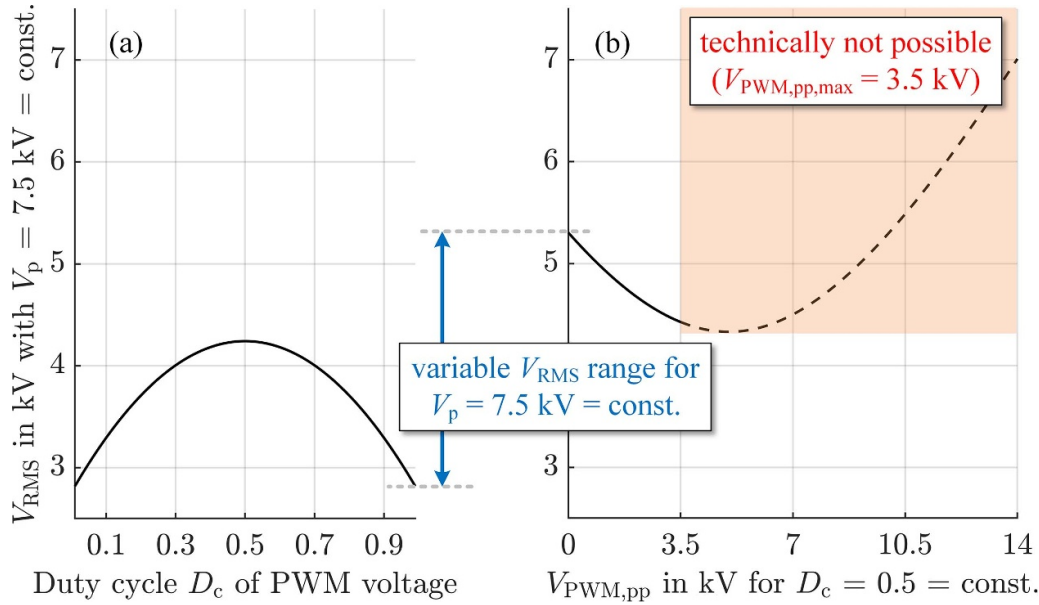
Figure 3. Possible variation range for RMS voltage stress V_{RMS} at constant peak voltage $V_p = 7.5\,kV$ by adjusting the duty cycle D_c (a) or the amplitude ratio between $V_{PWM,pp}$ and $V_{AC,p}$, i.e. $V_{AC,p}$ needs to be lowered according to an increased $V_{PWM,pp}$ (b).

standard conditions in table 2 in order to identify the individual influences of each parameter.

For PD-free aging, samples were stressed at either dry (RH = 0%) or high-humidity (RH = 75%) conditions as well as at either room temperature ($22\,°C \pm 1\,°C$) or $T = 70\,°C$. Note that the RH value exhibits an inaccuracy of $\pm 3\%$ according to the specifications of the RH sensor, whereas the temperature was found to be accurate within $\pm 1\%$. In addition, the influence of both the RMS and the peak voltage stress was studied, meaning it was necessary to vary V_{RMS}, while keeping V_p = const. and vice-versa. This can be achieved by a combination of two measures. First of all, the amplitude ratio of the two superimposed voltages $V_{AC,p}/V_{PWM,pp}$ can be varied as the total RMS voltage V_{RMS} is related to the total peak voltage V_p for a duty cycle $D_c = 0.5$ as follows:

$$V_{RMS} = \sqrt{(V_{AC,RMS})^2 + (V_{PWM,RMS})^2} \tag{1}$$

$$= \sqrt{\left(\frac{V_{AC,p}}{\sqrt{2}}\right)^2 + \left(\frac{V_{PWM,pp}}{2}\right)^2} \tag{2}$$

$$= \sqrt{\left(\frac{V_p - V_{PWM,pp}/2}{\sqrt{2}}\right)^2 + \left(\frac{V_{PWM,pp}}{2}\right)^2}. \tag{3}$$

Note that equation (1) is only true if the frequencies of $V_{AC,RMS}$ and $V_{PWM,RMS}$ do not share the same frequency components, which is the case in the present work since $f_{AC} = 50\,Hz < f_{PWM} = 1\ldots 40\,kHz$. The relation in equation (3) is shown for different $V_{PWM,pp}$ values and $D_c = 0.5$ = const. in figure 3 (right). Since, however, $V_{PWM,pp}$ is limited to 3.5 kV, the achieved variability is rather small (<20%). In order to extend the adjustable range, D_c can be changed in the range $0\ldots 1$. In the case of AC + PWM voltage stress, this leads to

the voltage maximum occurring either in the positive ($D_c < 0.5$) or in the negative ($D_c > 0.5$) half-wave of the sinusoidal voltage, as shown for the measured waveforms at two different duty cycles in figure 4. Note that the difference of the absolute values of the positive and negative peak PWM voltage for $D_c \neq 0.5$ is due to the coupling capacitor C_2 shown in figure 2, which eliminates a potential DC offset, resulting in a bipolar PWM voltage without a DC component. The total RMS voltage for variable D_c can be calculated as

$$V_{RMS}(D_c) = \sqrt{(V_{AC,RMS})^2 + [V_{PWM,RMS}(D_c)]^2} \tag{4}$$

$$= \sqrt{\left(\frac{V_{AC,p}}{\sqrt{2}}\right)^2 + \left(\sqrt{D_c(1 - D_c)} \cdot V_{PWM,pp}\right)^2}. \tag{5}$$

In figure 3(a), this relation is shown for different D_c values. From equations (3) and (5), the total variable V_{RMS} range is visible. In summary, varying of the RMS voltage V_{RMS} and keeping the peak voltage V_p = const. (and vice-versa) can be achieved by both changing the duty cycle D_c and adjusting the amplitude ratio $V_{AC,p}/V_{PWM,pp}$ accordingly.

In order to investigate whether the polarity of the maximum voltage stress has an influence, measurement series for both peak voltage polarities were carried out. Furthermore, the influence of the type of MF voltages was studied by aging at either pure AC, DC or PWM voltage stress as well as at AC + PWM and DC + PWM voltage stress. In addition, the influence of PWM frequency, slew rate and aging time was investigated. The slew rate was varied by changing the value of resistor R_2 shown in figure 2, which results in a different rise time τ_r due to the changed time constant $\tau_{RC} = (R_1 + R_2) \cdot (C_2^{-1} + C_{DUT}^{-1})^{-1}$ for charging the total load capacitance. The measured rise times τ_r (defined from 10% to 90% of $V_{PWM,pp}$)
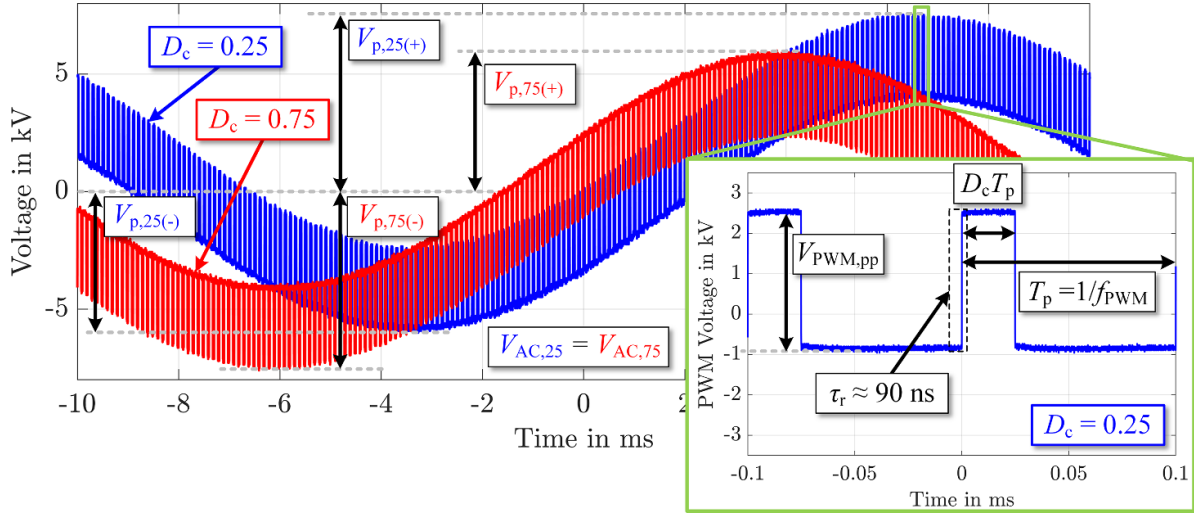
Figure 4. Example of measured mixed-frequency medium-voltage (MF-MV) waveforms composed of the same AC (50 Hz) voltage, but different superimposed PWM (10 kHz) voltages (due to different duty cycles D_c), which leads to different peak voltages in the positive (+) and negative (−) half-waves. The two waveforms are phase-shifted for better visibility.

Table 2. Standard voltage and ambient stress parameters used in this work (if not stated otherwise for a measurement series) for aging with silver-coated electrodes in the PD-free regime (I) as well as without silver-coated electrodes in the PD-free regime (II) and in the PD stress regime (III).

Aging regime	$V_{AC,p}/V_{PWM,pp}/f_{PWM}/D_c$ in kV/kV/kHz/—	$V_{PWM,pp}/\tau_{r,l}$ in kV μs^{-1}	V_p in kV	V_{RMS} in kV	t_d in h	T in °C	RH in %
I	5.75/3.5/10/0.5	38.9	7.5	4.4	48	22 ± 1	75 ± 3
II	0/2/10/0.5	38.9	1	1	0.5	22 ± 1	75 ± 3
III	6.5/2/10/0.5	38.9	7.5	4.7	0.5	22 ± 1	75 ± 3

for $V_{PWM,pp} = 3.5\,\text{kV}$ and two different resistors R_2 (90.3 Ω or 102.2 kΩ) were $\tau_{r,l} \approx 90\,\text{ns}$ and $\tau_{r,h} \approx 23.3\,\mu s$, which resulted in slew rates of $38.9\,\text{kV}\,\mu s^{-1}$ and $0.15\,\text{kV}\,\mu s^{-1}$, respectively. The higher rise time $\tau_{r,h}$ led to a rise of the PWM voltage which was too slow to reach the full peak-to-peak PWM voltage $V_{PWM,pp}$ within one PWM half-cycle for the standard test frequency $f_{PWM} = 10\,\text{kHz}$. Thus, the frequency for the comparison of different slew rates was chosen as $f_{PWM} = 1\,\text{kHz}$ which was sufficient to reach $V_{PWM,pp}$ within one PWM half-cycle due to the ten times longer pulse width.

Another exception from the standard test conditions listed in table 2 is the lower PWM voltage $V_{PWM,pp} = 2\,\text{kV}$. The reduction in voltage was necessary for PWM frequencies larger than 10 kHz due to the thermal limits of the used metal-oxide-semiconductor field-effect transistor (MOSFET) switch, as the generated switching losses $P_{l,PWM}$ are related to the switching frequency and voltage according to

$$P_{l,PWM} \propto V_{PWM,pp}^2 \cdot f_{PWM}. \qquad (6)$$

In order to keep the total peak voltage in this case constant at $V_p = 7.5\,\text{kV}$, the AC peak voltage was chosen as 6.5 kV for aging sequences with $f_{PWM} > 10\,\text{kHz}$.

In case of a breakdown occurring before the intended end of an aging sequence, the silver coating of the failed sample was removed with ethanol and the sample surface was optically examined for traces of PD erosion. It was observed that

all of the few samples with PD traces failed within 10 h of aging, while failures of samples without PD traces occurred always after longer aging times. The results of this investigation are found in [16]. Furthermore, optical analysis of non-failed samples after 48 h of aging consistently revealed no PD traces. This confirms the absence of PDs for samples aged for the standard aging time of 48 h. All the failed samples were replaced with new ones, which were then aged individually to obtain the same aging time for all samples. However, as sample failures during PD-free aging represent a clear sign of (rather strong) aging, the number of failed samples per stress condition was compared to the results of non-destructive aging analysis to study potential correlations.

For non-coated electrodes, measurements were conducted at dry (RH = 0%) and high-humidity (RH = 75%) conditions below and above the PDIV (see table 2), which was determined as described in section 2.3. In addition, measurements were carried out at two different V_p levels above the PDIV. These two levels differed in values of $V_{AC,p}/V_{PWM,pp}$ and D_c, whereas $V_{RMS} = \text{const}$. After the PD-related aging, samples were silver-coated in order to conduct further aging analysis as described in section 2.5.

2.5. Aging evaluation

The health state of the epoxy samples was examined in the same way before and after each MF-MV aging sequence. For
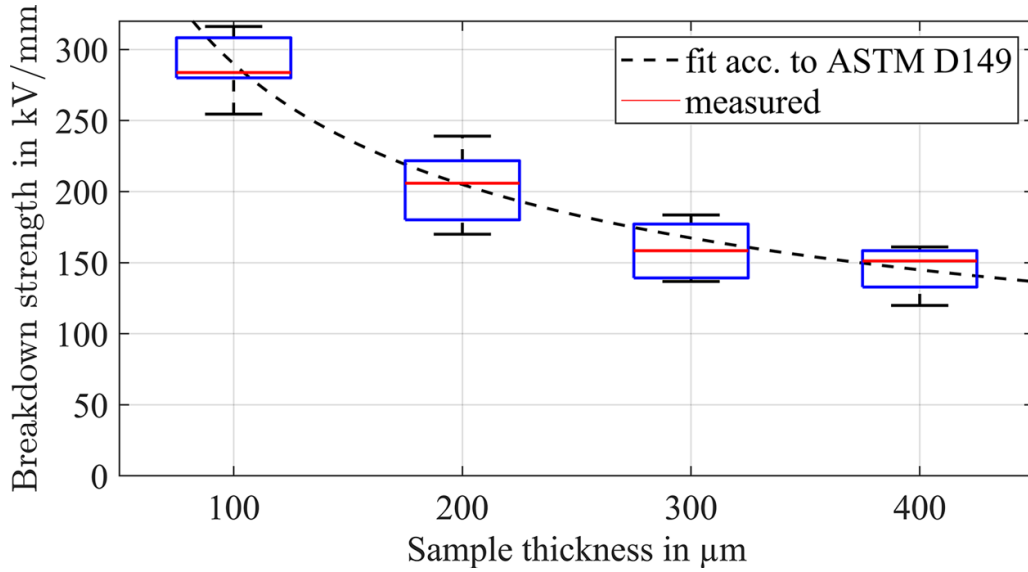
Figure 5. Comparison between measured short-term AC breakdown strength for different non-aged epoxy sample thicknesses and fitted values according to equation (7) from ASTM D149 [67].

this purpose, several potential aging markers were tested for their suitability to reveal evidence of aging as well as information about the underlying aging mechanisms. If samples were aged at humid conditions, they were dried before the aging analysis at RH = 0% for >48 h at room temperature in order to focus on irreversible aging effects instead of reversible effects due to the presence of water. The potential aging markers evaluated in this work are the short-term AC (50 Hz) breakdown strength, the relative permittivity (real and imaginary part), the DC volume resistivity, the glass transition temperature T_g as well as the characteristic spectra from FTIR measurements. Note that except for breakdown strength and T_g measurements (which both are destructive methods), the same set of samples were tested before and after aging. The breakdown strength and T_g was measured on two identically manufactured and pre-conditioned sets of samples (out of which one set consisted of non-aged and one set of aged samples).

The short-term AC breakdown strength was measured according to IEC 60243-1 and ASTM D149 with a voltage ramp of $2\,kV\,s^{-1}$ to reach the breakdown in typically $10\ldots20\,s$ [66, 67]. For this purpose, an AC (50 Hz) voltage was applied at the samples, which were immersed in insulating oil (Shell Diala S4 ZX-1) to prevent surface discharges. The volume/thickness effect was considered by relating the measured breakdown strength $V_{bd,m}$ for each measured thickness $d_m \in [190\,\mu m, 210\,\mu m]$ to the value at $200\,\mu m$ by [67]

$$V_{bd,200\,\mu m} = \sqrt{\frac{200\,\mu m}{d_m}}\,V_{bd,m}. \qquad (7)$$

This relation was verified by measurements of non-aged epoxy samples with different thicknesses, see figure 5. However, the maximum voltage differences according to equation (7) for the samples used in this work were below 5% and thus almost negligible. The measured breakdown strength data is represented as box plots, consisting of median (red line in figure 5),

boxes between the 25th and 75th percentiles (blue boxes) with whiskers (black lines) up to 1.5 times the interquartile distance. Values outside of this range are separately shown as outliers, which occurred, however, very rarely.

The complex relative permittivity, namely its real (ε_r') and imaginary (ε_r'') part was determined by means of a broadband dielectric spectroscopy (BDS) measurement setup. The description of the setup and the measurement procedure can be found in [16, 35, 62, 68]. Note that within the present work, the silver electrodes used during aging were removed with ethanol and new silver electrodes were applied only at the inner part of the sample in order to probe only the dielectric response of the flat part of the sample after aging.

Polarization-depolarization current (PDC) measurements allowed the estimation of the (apparent) volume DC resistivity by measuring the current difference between the polarization and depolarization current components after 1 h, which is related to the apparent DC resistivity as described in [69]. Measurements were performed at RH = 0% and at an elevated temperature of 90 °C to obtain current signals that were sufficiently above the noise level. The experimental procedure is explained in detail in [16].

Glass transition temperature measurements were carried out by means of differential scanning calorimetry (DSC) with a Mettler Toledo DSC 1 device. In the case of aged samples, the silver electrodes were removed with ethanol before each measurement. Measurements were always carried out with material extracted from the flat part of the samples, i.e. where the highest electrical stress was applied during the aging. A heating rate of $10\,K\,min^{-1}$ in the range $25\,°C\ldots180\,°C$ with two cycles per sample was chosen for all measurements.

FTIR was used to analyze the chemical composition of the non-aged and aged samples. Measurements were carried out with a diamond attenuated total reflection type device (Varian 640 Fourier Transform Infra Red Spectrometer) in the wavelength range $750\ldots4000\,cm^{-1}$. For aged samples, the

J. Phys. D: Appl. Phys. **56** (2023) 354005

F Küchler *et al*

silver electrodes were removed with ethanol before each FTIR scan. Note that the absorbance around 1608 cm^{-1} is reported to be relatively stable and unaffected by aging due to its correspondence to the aromatic structure in epoxy [70]. It was thus used as the `reference peak for all FTIR measurements.

More detailed descriptions of the measurement procedures and used setups can be found in [16]. Therein, it was found that only the short-term AC breakdown strength is sensitive to aging effects. Consequently, the focus in the present contribution is on this promising aging marker. The aging markers previously identified as insensitive to the applied dielectric aging (measured by BDS, PDC, DSC, FTIR) were not investigated for all, but only for one out of eight aged samples in order to have enough samples for the (destructive) breakdown strength testing.

3. Results

In the following section, the aging evaluation results for samples stressed under different conditions in the presence as well as in the absence of PDs are presented.

3.1. Aging in the presence of PDs

First of all, the measurement results of the PDIV are shown and thereafter, the short-term AC breakdown strength of the samples aged under different stress conditions in the presence of PDs are presented.

3.1.1. Results of PDIV measurements. The PDIV measurements performed according to the procedure described in section 2.3 resulted in the values shown as box plots in figure 6. Compared to the dry (D) conditions, the PDIV values at high humidity (H) are slightly lower and show less (to no) scatter at 50 and 1000 Hz. Clearly, the PDIV demonstrates a rising tendency with the test voltage frequency for both condition types. Using these results, the limits for the aging in the presence and absence of PDs can be set: below $\approx$1100 V(peak), PDs should not be occurring, as the test voltage is below the lowest measured PDIV at 50 Hz (the frequency trend increases monotonously, suggesting that the PDIV of the PWM pulses should be higher than that of 50 Hz). Above $\approx$1600 V(peak), the PDs appear within a very short time after the application of the test voltage, ensuring their presence for the entirety of the chosen aging time. For the investigations of this work, however, even lower and higher voltage levels were applied for aging below and above the PDIV, respectively (see table 2). Note that aging below the PDIV was thus investigated for non-coated samples as described in this section as well as for silver-coated samples with the results being described in section 3.2.

PRPD patterns of the PD activity at 50 Hz and 7.5 kV(peak) were constructed for each condition type, as depicted in figure 7. Both patterns show that the PD events occur roughly between $340°\ldots100°$ and $145°\ldots285°$, respectively, i.e. approximately between the test voltage zero-crossings and peak values. Furthermore, compared to the high humidity conditions, the PD activity under the dry conditions seems to be
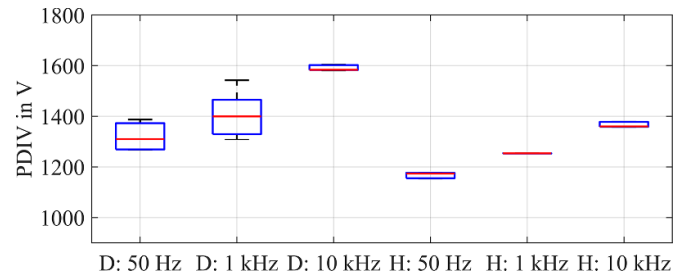

Figure 6. Partial discharge inception voltage (PDIV) for non-coated sample surface and sphere-to-plate electrodes and a sinusoidal voltage of different frequencies under dry (D: RH = 0%) and humid (H: RH = 75%) conditions, with five measurements at each condition.

substantially less frequent (by a factor of about five per the PD count), whereas the discharges appear to be significantly stronger (about four times stronger on average per the I_{AVG}).

3.1.2. Influence of aging conditions. Breakdown strength measurements of non-coated epoxy samples, aged below the PDIV, led to no significant changes at both dry (D: RH = 0%) and high-humidity (H: RH = 75%) conditions, see figure 8. However, measurements above the PDIV consistently led to a reduced breakdown strength. The reduction was stronger if aging was carried out at high RH level. In addition, the results indicate stronger aging at higher peak voltage stress (for the same RMS voltage stress). The polarity of the maximum voltage stress was found to play no role in terms of aging effects.

Visual inspection of samples revealed that only samples stressed in the presence of PDs showed circular traces of PD erosion around the location where the spherical electrode was placed. In contrast, no visual differences between non-stressed and stressed samples could be observed if the electrical stress was below the PDIV.

3.2. Aging in the absence of PDs

In this section, the results of aging in the absence of PDs are presented. Firstly, the short-term AC breakdown strength E_{bd} measurements of silver-coated samples aged under different types of stress conditions are shown. These breakdown strengths are afterward compared to those of the prematurely failed samples (i.e. before the intended end of aging) in order to evaluate potential correlation between breakdown strength and lifetime measurement results. In the last step, the measurement results of the other investigated potential aging markers are described, but less extensively, as it was found in an earlier work [16] that they were not sensitive to the dielectric aging revealed by the decrease in the short-term breakdown strength.

3.2.1. Influence of RH. As depicted in figure 9, no significant changes in the breakdown strength were observed after aging at dry conditions (RH = 0%) over a broad range of V_{RMS} values (for $V_{\mathrm{p}} = \mathrm{const.}$). For measurements with

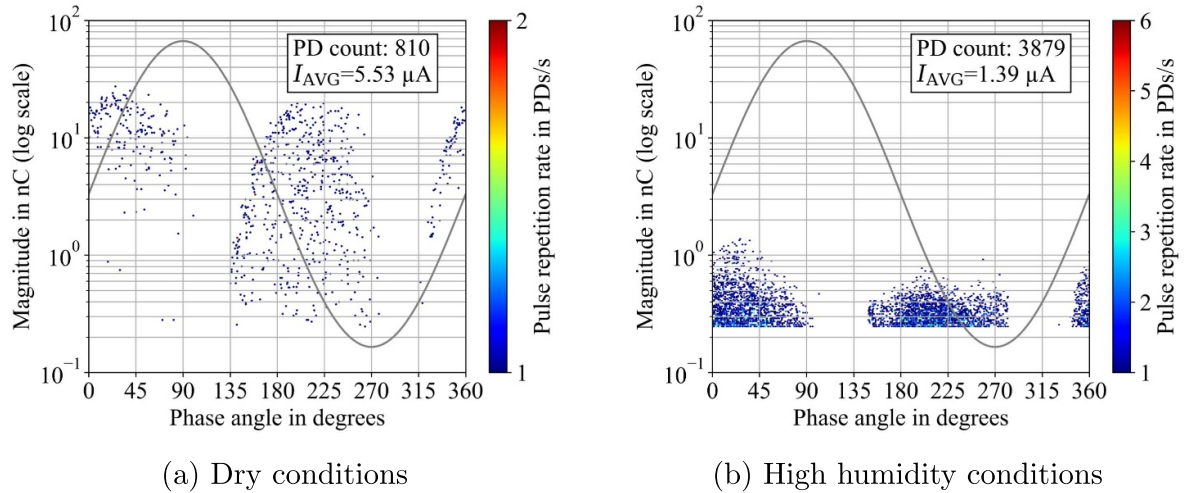(a) Dry conditions (b) High humidity conditions

Figure 7. PRPD patterns of discharge activity obtained at 7.5 kV (peak), 50 Hz under humid and dry conditions. I_{AVG} is the average discharge current calculated according to IEC 60270 [63]. The series capacitor PD instrument was calibrated prior to the measurement, resulting in a scaling factor of about 1.6 nC/1 V, where the voltage refers to the height of the voltage jumps.
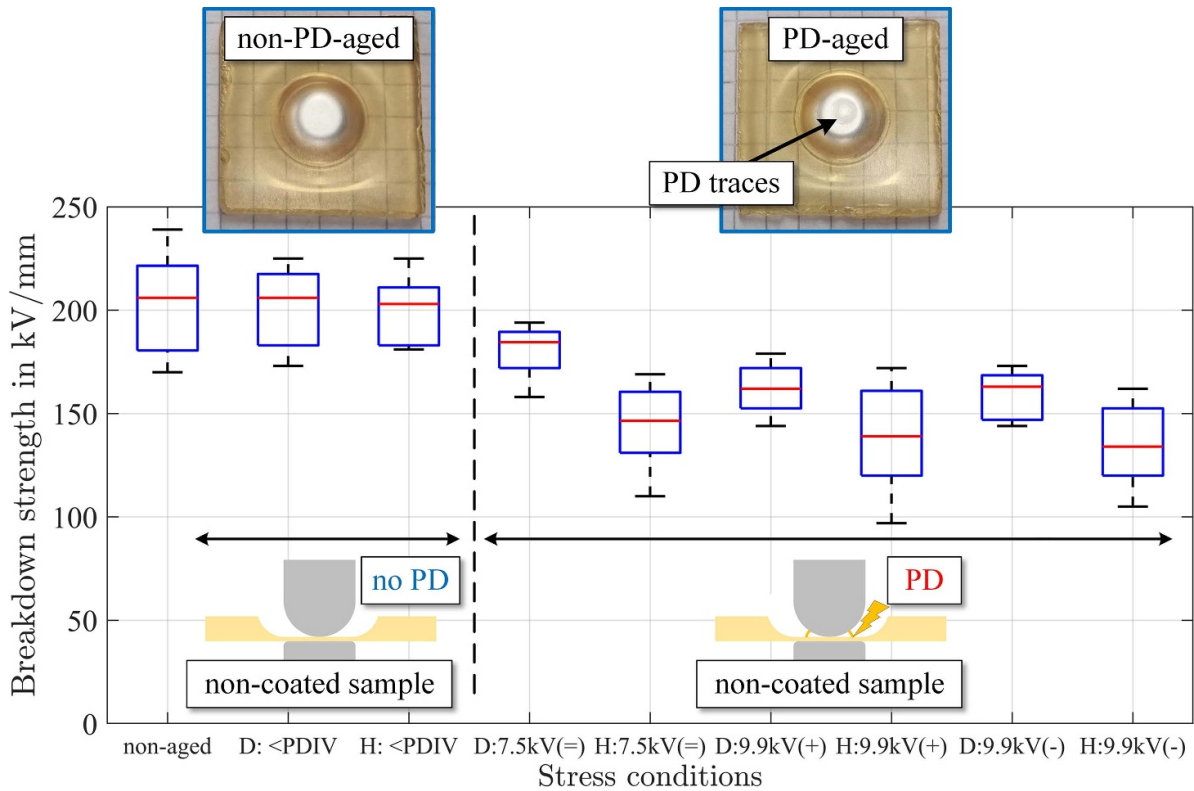

Figure 8. Short-term AC breakdown strength results of non-aged and aged (for 0.5 h) epoxy samples with sphere-to-plate electrodes and non-coated sample surfaces below and above the PDIV at dry (D) or humid (H) conditions (see electrical aging conditions in table 2). Aging above the PDIV was carried out at $V_{RMS} =$ const. and the listed different V_p values with the voltage maximum occurring either in the positive (+), negative (−) or equally in both half-waves (=). Pictures of samples aged in the absence (left) and in the presence (right) of PD activity are shown in the top part, whereas it needs to be mentioned that the samples are shown from below after the bottom layer of silver paint was removed (in order to make the PD traces visible).

samples aged under the same electrical stress conditions, but at high humidity (RH = 75%), a clear decrease of E_{bd} is visible in figure 10. This decrease is stronger, the higher the applied RMS voltage stress was, an observation, which is taken up again in section 3.2.3.

In addition, the isolated influence of humidity (in the absence of the electric field), i.e. saturated (steady-state) water absorption inside the sample volume, was investigated. The breakdown strength results after aging at RH = 75% for either 120 h or 1440 h (the samples aged for 120 h were not dried
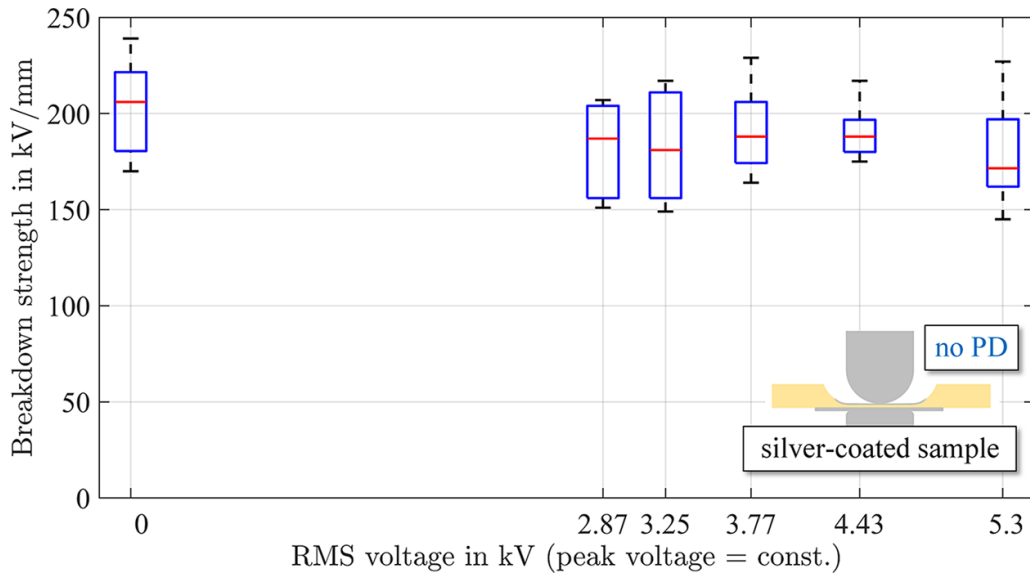
Figure 9. Short-term AC breakdown strength results of non-aged and aged (AC + PWM stress) epoxy samples under RH = 0% with $V_p = 7.5\,\mathrm{kV} = \mathrm{const.}$ (maximum peak in positive half-wave, i.e. $D_c < 0.5$) and variable V_{RMS}. The value at $V_{RMS} = 5.3\,\mathrm{kV}$ corresponds to pure AC stress.
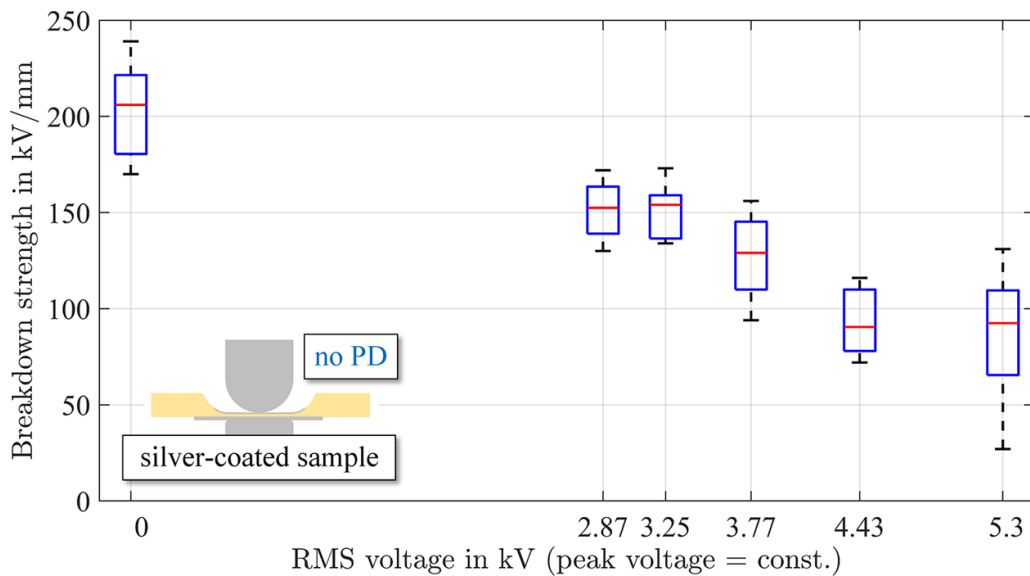

Figure 10. Short-term AC breakdown strength results of non-aged and aged (AC + PWM stress) epoxy samples under RH = 75% with $V_p = 7.5\,\mathrm{kV} = \mathrm{const.}$ (maximum peak in positive half-wave, i.e. $D_c < 0.5$) and variable V_{RMS}. The value at $V_{RMS} = 5.3\,\mathrm{kV}$ corresponds to pure AC stress.

prior to the breakdown strength testing) as well as the results for hygrothermally (95 °C in de-ionized water for 168 h) aged samples are shown in figure 11 together with pictures of the non-aged and aged samples. It is evident that neither of these conditions (labeled with an 'H'/'HT') led to aging with respect to E_{bd} or the optical appearance of the epoxy samples.

3.2.2. Influence of temperature. Analogously to the pure humidity stress, the isolated influence of temperature stress on the breakdown strength was studied. The respective findings

of samples aged at 90 °C, 160 °C (both for 120 h) as well as at 190 °C (for 168 h) are also shown in figure 11 together with corresponding pictures of non-aged and aged samples. As visible from these results (data sets labeled with an 'T'), the breakdown strength decreases with increasing aging temperature. This trend correlates with optical changes of the samples, as they became significantly darker during aging at high temperatures. It also correlates with thickness changes, since the average sample thickness measured after aging was reduced by 25.5%.

Thermoelectrical aging at 70 °C, dry conditions and three different types of electrical stress conditions resulted in the
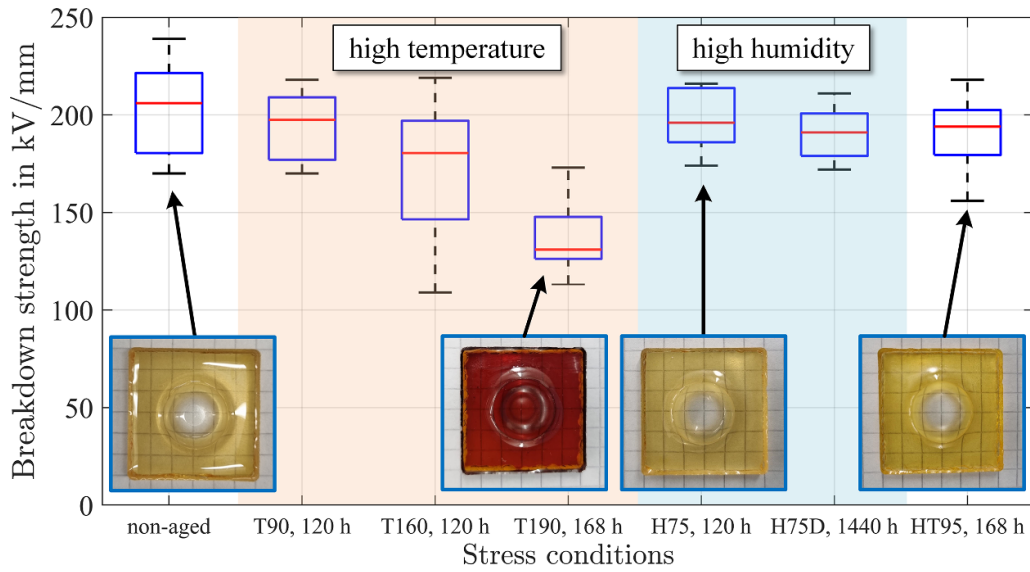
Figure 11. Short-term AC breakdown strength results with pictures of non-aged and aged epoxy samples, which were stressed without electric field under either pure thermal (T), pure humidity (H) or hygrothermal (HT) stress for specific amounts of time, whereas the number after the stress-type indicator is either the corresponding temperature in $^{\circ}C$ or the relative humidity in %. A set of samples was dried (D) after pure humidity stress and hygrothermal stress was carried out at 95 $^{\circ}C$ in a de-ionized water bath.
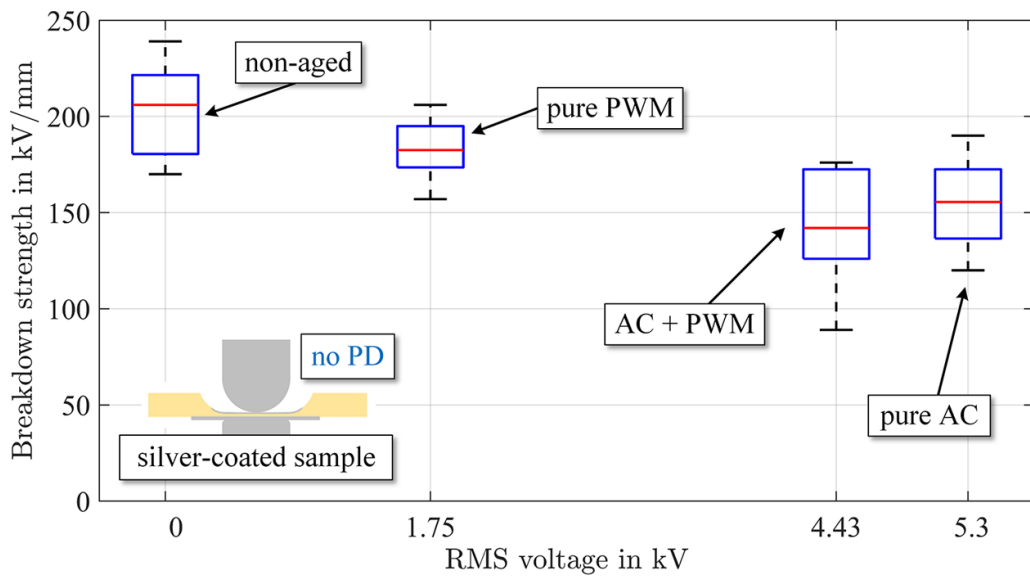

Figure 12. Short-term AC breakdown strength results of non-aged and thermoelectrically aged epoxy samples, which were aged under different types of voltage waveforms at 70 $^{\circ}C$ and dry conditions.

breakdown strength values shown in figure 12. While for pure PWM stress, only a slight reduction in the breakdown strength was observed, a stronger reduction occurred for AC + PWM as well as for pure AC stress. However, it should be noted that the RMS voltage stress was different for the three types of voltage waveforms. Another observation during execution of measurements at elevated temperatures was the increasing risk of electrode delamination even at temperatures below 125 $^{\circ}C$, which is the maximum applicable temperature of the silver conductive paint according to [71]. Nevertheless, electrode delaminations were not observed at the conditions used for the measurements shown in figure 12. This was further confirmed by removing the silver electrodes with ethanol and inspecting of

the sample surface for potential PD traces, which were not found on any sample.

3.2.3. Influence of RMS voltage stress. As already shown in figure 10 for AC + PWM stress, a clear dependence of the breakdown strength on the RMS voltage stress was found for constant peak voltage stress at high humidity, but not at dry conditions at ambient temperature (figure 9). A similar study was conducted for pure PWM stress, whereas the RMS and peak voltage stress is equal for bipolar PWM waveforms with $D_c = 0.5$. The results shown in figure 13 also indicate a dependence on $V_{RMS} = V_p = V_{PWM,pp}/2$.
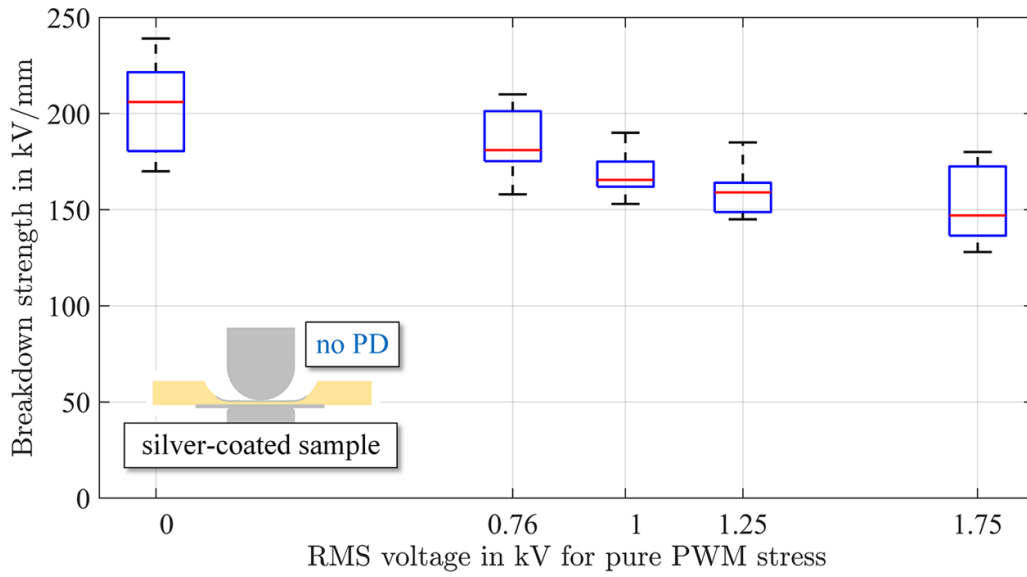
J. Phys. D: Appl. Phys. **56** (2023) 354005

F Küchler *et al*

Figure 13. Short-term AC breakdown strength results of non-aged and aged epoxy samples under pure PWM stress at RH = 75% and variable $V_{\text{RMS}} = V_{\text{p}} = V_{\text{PWM,pp}}/2$.
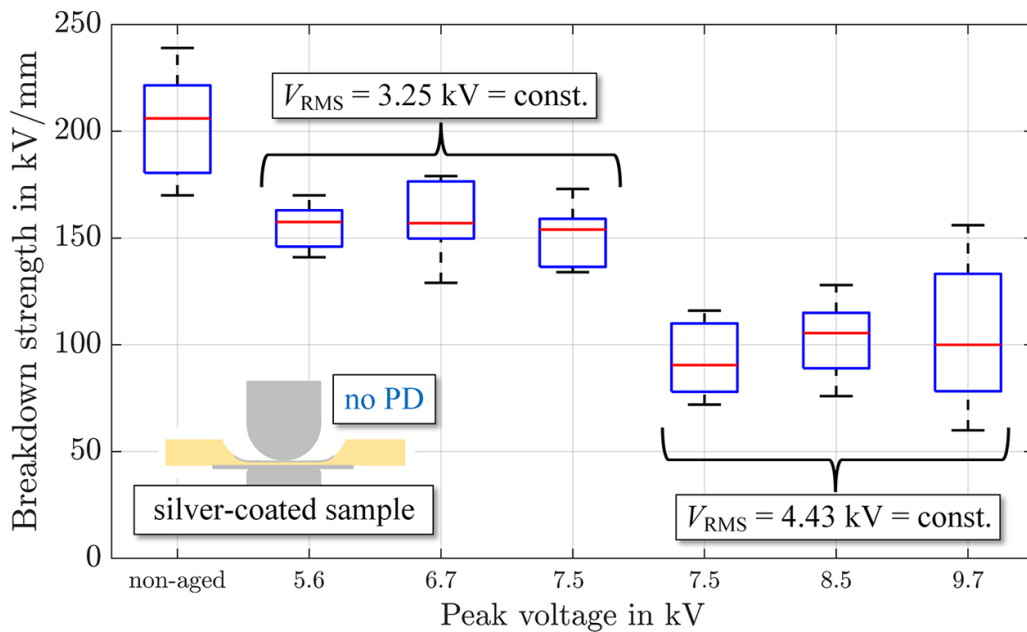

Figure 14. Short-term AC breakdown strength results of non-aged and aged (AC + PWM stress) epoxy samples under RH = 75% with two levels of $V_{\text{RMS}} = $ const. and variable V_{p}.

3.2.4. Influence of peak voltage stress. Analogous to the method described in section 2.4, the peak voltage can be varied, while keeping the RMS voltage constant. This was done for two different RMS voltage stress levels and resulted in the breakdown strength measurements displayed in figure 14. It can be seen that the peak voltage stress has no significant effect on E_{bd}, in contrast to the RMS voltage stress (in the presence of water).

3.2.5. Influence of polarity of maximum peak voltage stress. The maximum peak voltage stress occurred, depending on the duty cycle, either in the positive or in the negative half-wave of the sinusoidal voltage, see section 2.4. As a consequence, a study on the effect of the polarity of the maximum voltage stress was carried out at different RMS voltage stress levels and RH = 75%. The short-term AC breakdown strength results for the maximum voltage stress during aging occurring
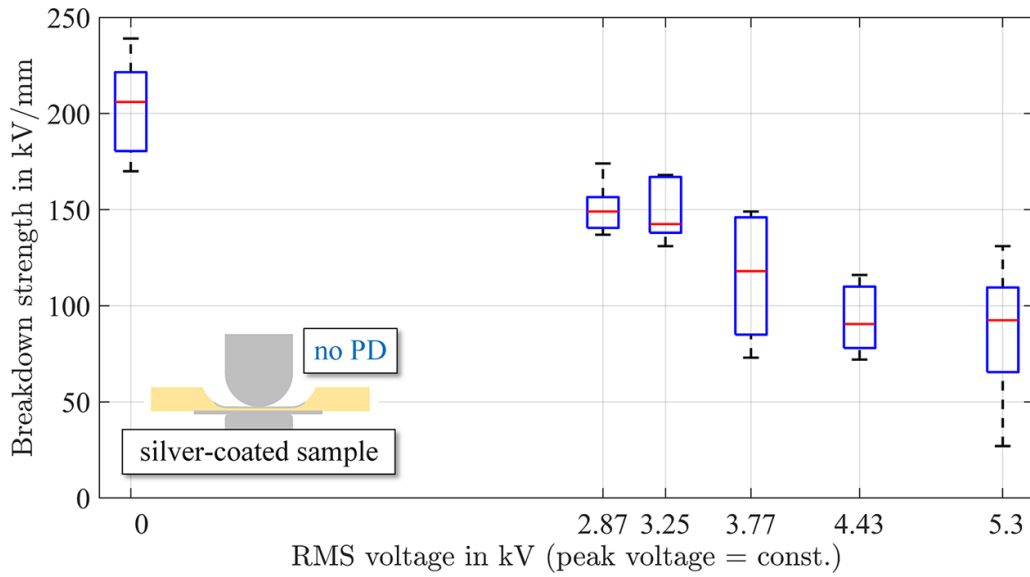
Figure 15. Short-term AC breakdown strength results of non-aged and aged (AC + PWM stress) epoxy samples under RH = 75% with $V_p = 7.5$ kV = const. (maximum peak in negative half-wave, i.e. $D_c > 0.5$, in contrast to $D_c < 0.5$ in figure 10) and variable V_{RMS}. The value at $V_{RMS} = 5.3$ kV corresponds to pure AC stress.
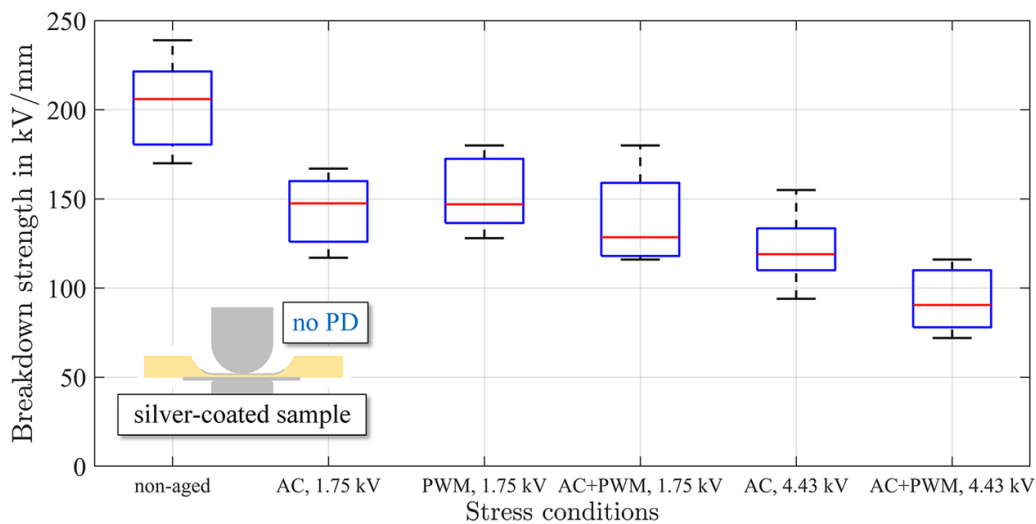

Figure 16. Short-term AC breakdown strength results of non-aged and aged epoxy samples, which were stressed at RH = 75% with either pure AC (50 Hz), pure PWM (10 kHz) or combined AC + PWM voltage stress at $V_{RMS} = 1.75$ kV or $V_{RMS} = 4.43$ kV.

in the positive half-wave were already shown in figure 10, whereas the corresponding results for the maximum voltage stress (absolute value) occurring in the negative half-wave are displayed in figure 15. Comparison of both studies confirm that no influence of the polarity of the maximum voltage stress exists.

3.2.6. Influence of type of MF-MV waveform. A comparison of differently composed MF-MV waveforms (either pure AC, pure PWM or AC + PWM) used for aging at two RMS voltage stress levels is shown in figure 16. The frequency of the AC voltage was 50 Hz, whereas the switching frequency of the PWM voltage was 10 kHz. The results indicate no significant

influence of the type of voltage waveform whenever just one type of voltage is present (i.e. either pure AC or pure PWM), but a slightly stronger reduction in breakdown strength was observed for MF voltages (AC + PWM) compared to single-frequency voltages, especially for $V_{RMS} = 4.43$ kV.

In addition to the alternating electric field stress, also pure DC as well as DC + PWM electrical stress conditions were investigated at RH = 75%. The results are displayed in figure 17 together with an overview of the results for other types of voltage stresses (pure PWM, pure AC, AC + PWM) described so far. As seen from this representation, pure DC stress leads to no change in the breakdown strength, despite its high RMS voltage stress. If, however, a PWM voltage is superimposed onto the DC voltage (with $V_p =$ const.), a
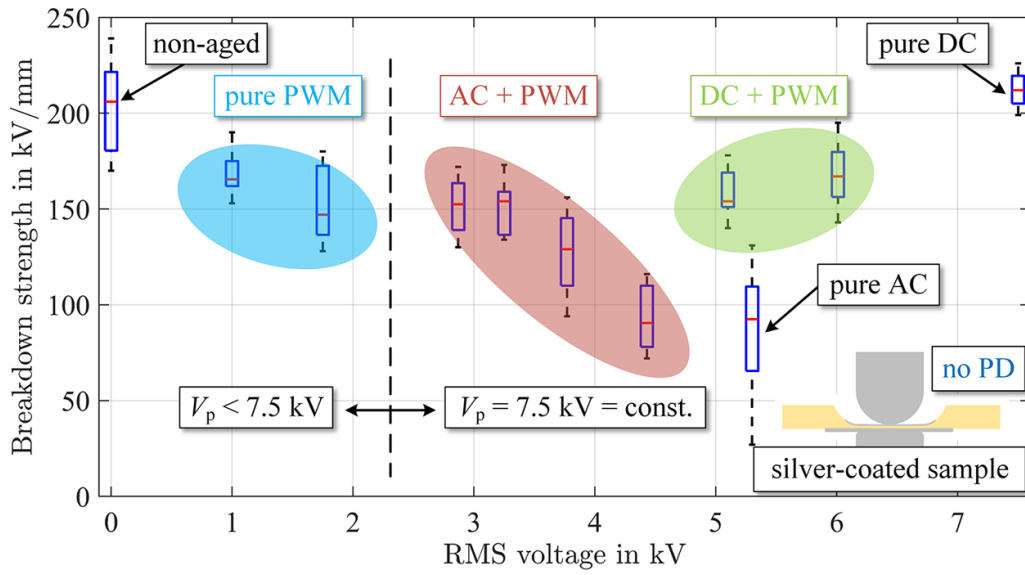
Figure 17. Short-term AC breakdown strength results of non-aged and aged epoxy samples, which were stressed at RH = 75% with different superimposed voltage forms and variable V_{RMS}.
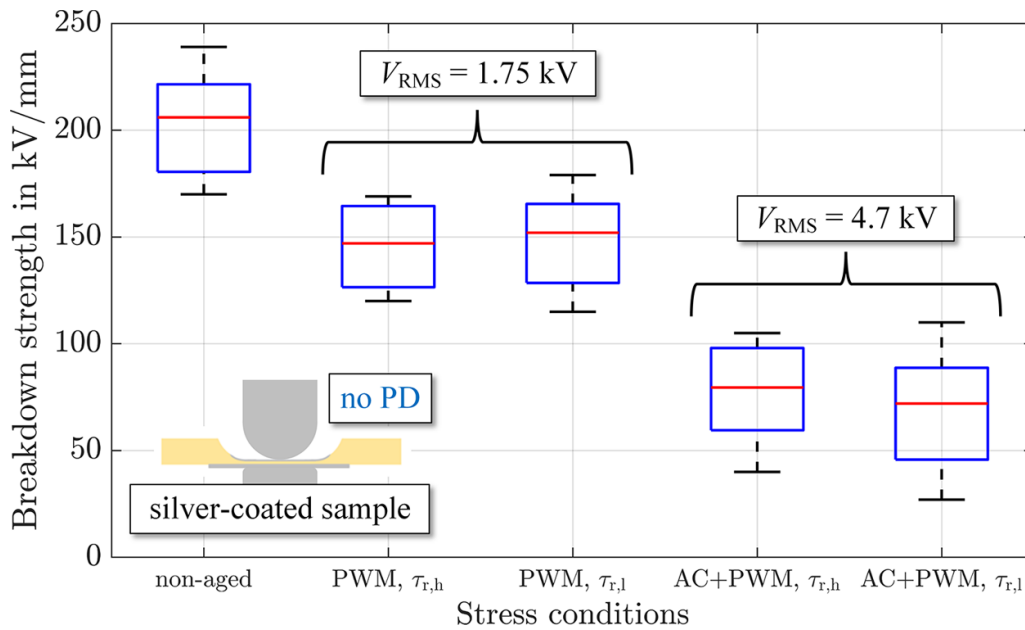

Figure 18. Short-term AC breakdown strength results of non-aged and aged epoxy samples at RH = 75% under the same electrical stress conditions for pure PWM stress as well as AC + PWM stresses with two different rise times $\tau_{r,l} \approx 90$ ns and $\tau_{r,h} \approx 23.3\,\mu$s (i.e. different slew rates of the PWM voltage) and different RMS voltage values.

similar reduction in E_{bd} as for pure PWM voltage stress is observed. All in all, the breakdown strength data presented in figure 17 provides a summary of the main observations from the aging studies with a focus on the different degrees of aging for each type of voltage waveform.

3.2.7. Influence of slew rate of PWM voltage. Aging under the same hygroelectrical stress conditions, but with two different rise times $\tau_{r,l} \approx 90$ ns and $\tau_{r,h} \approx 23.3\,\mu$s (i.e. two different slew rates) led to the short-term AC breakdown strength results shown in figure 18. It is evident that for both pure PWM stress as well as for AC + PWM stress, a similar reduction in

E_{bd} results for both tested slew rates. The difference between the different types of voltage waveforms is mainly attributed to the different RMS voltage values, see section 3.2.3.

3.2.8. Influence of PWM frequency stress. As it was found in the previous section that only alternating electric field stress led to significant changes in the breakdown strength, the influence of the PWM switching frequency was studied for both for AC + PWM voltage stress as well as for pure PWM voltage stress. The results of aging under AC + PWM voltage stress are shown in figure 19, whereas aging under
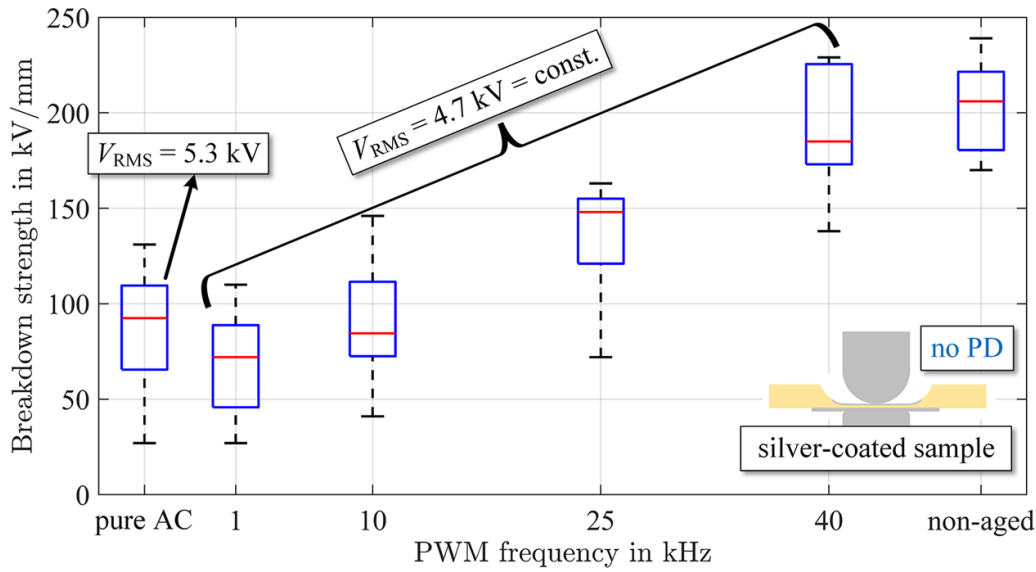
Figure 19. Short-term AC breakdown strength results of non-aged and aged (AC + PWM stress) epoxy samples under RH = 75% with $V_p = 7.5$ kV = const. and variable PWM frequency.
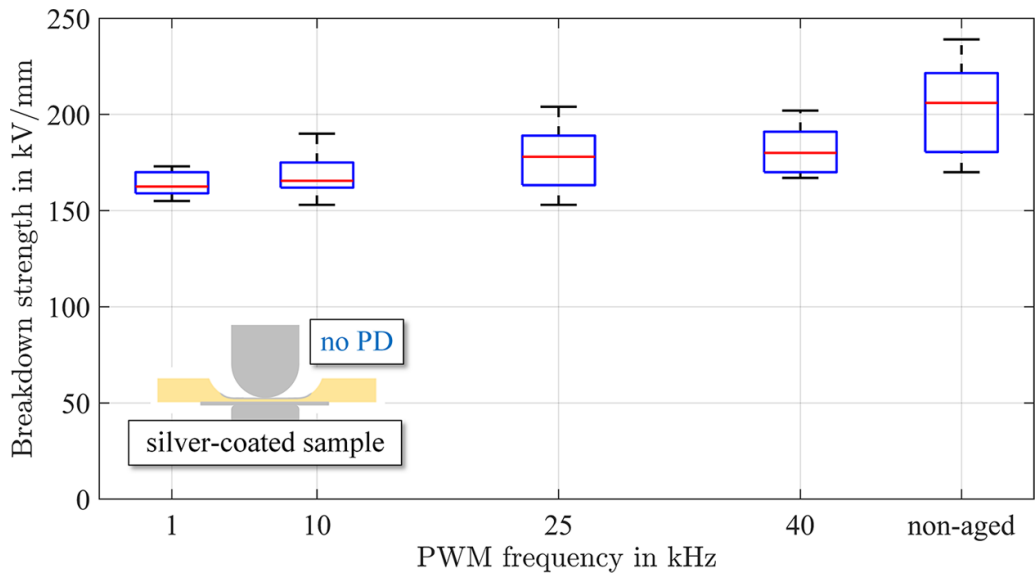

Figure 20. Short-term AC breakdown strength results of non-aged and aged (pure PWM stress) epoxy samples under RH = 75% with $V_{RMS} = V_{PWM,pp}/2 = 1$ kV = const. and variable PWM frequency.

pure PWM voltage stress resulted in the E_{bd} values displayed in figure 20. In both cases, the lower the applied PWM frequency was, the stronger the reduction in breakdown strength became. Note that only minor changes in E_{bd} were measured for the highest PWM frequency of 40 kHz. For AC + PWM stress with $f_{PWM} = 1$ kHz, the breakdown strength was reduced slightly more compared to pure AC stress even if the RMS voltage was slightly lower (4.7 kV compared to 5.3 kV). This observation is similar to the stronger E_{bd} reduction for an MF voltage compared to a single-frequency voltage shown in figure 16. Overall, the reduction in breakdown strength is much stronger if the superimposed AC voltage was present, which is attributed to the higher total RMS voltage stress, see section 3.2.3.

3.2.9. Influence of aging time. Investigations on the time of applied MF-MV stress at RH = 75% led to the results shown in figure 21. It can be seen that an apparent reduction in breakdown strength started to manifest between 0.5...5 h of aging and increased with longer aging times.

3.2.10. Comparison between early sample failures and breakdown strength. As mentioned above, during some of the investigated aging sequences, sample failures occurred before the intended end of aging, i.e. <48 h. These samples were replaced by new ones, which were subsequently aged individually to obtain the same aging time for all eight samples. In figure 22, the measured breakdown strength reduction after
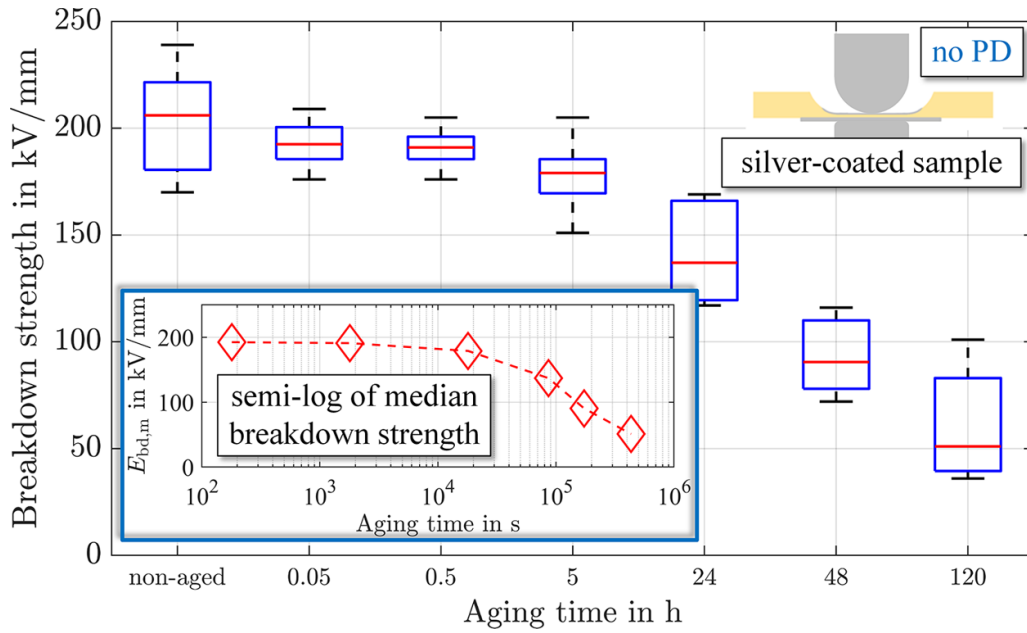
Figure 21. Short-term AC breakdown strength results of non-aged and aged (AC + PWM stress) epoxy samples for different aging times at RH = 75% with a semi-log representation of the median breakdown strength $E_{bd,m}$ over the aging time.
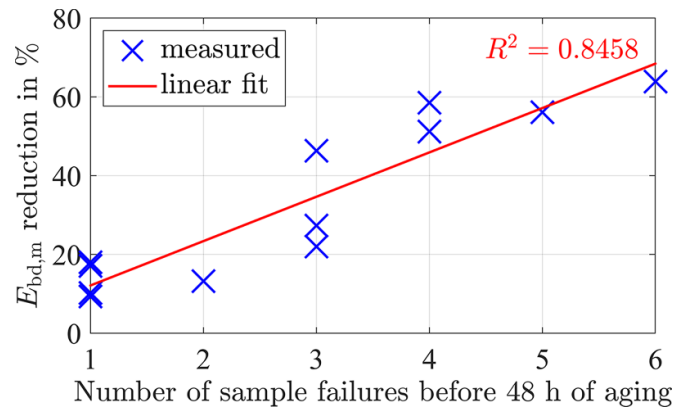

Figure 22. Comparison between the reduction of the short-term AC breakdown strength (median) and the number of silver-coated samples failed before the intended end (i.e. before 48 h) of the respective PD-free aging sequence (out of all different aging sequences studied in this work).

PD-free aging, namely the reduction of its median value $E_{bd,m}$ (of in total eight samples), is displayed together with the corresponding number of failed samples during aging at the respective aging sequence. A linear fit of the data shows the correlation between the breakdown strength and the number of sample failures, which is quantified by the coefficient of determination, calculated as $R^2 = 0.8458$.

3.2.11. Evaluation of potential aging markers. A systematic study on other potential aging markers than the short-term AC breakdown strength was conducted after aging under the most severe stress conditions found from the E_{bd} measurements described above. The strongest reduction in breakdown strength was observed at the PD-free aging conditions listed in table 2. Measurements of the complex relative permittivity (real and imaginary part), volume DC resistivity, glass transition temperature and FTIR spectra according to section 2.5, however, revealed no significant changes. The detailed measurement results can be found in a former work [16].

4. Discussion

In the following section, the obtained results are discussed in different subsections.

4.1. PD inception

The observed rising tendency of the PDIV of non-coated samples with increasing frequency (up to 10 kHz) of the sinusoidal test voltage can be explained on the basis of
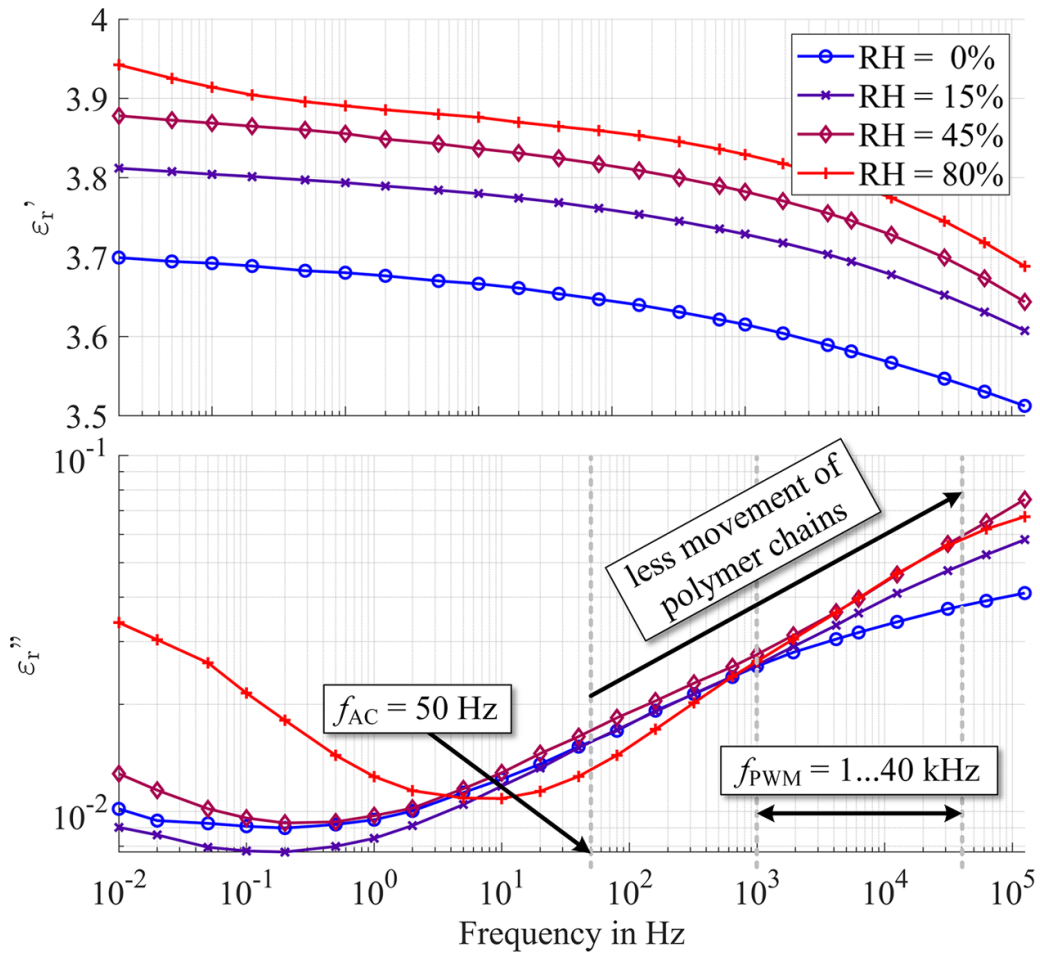
Figure 23. Dependence of real (top) and imaginary (bottom) part of the complex relative permittivity on frequency of non-aged epoxy samples at 10 °C and different levels of relative humidity (RH).

the frequency dependence of the epoxy samples' relative permittivity ε_r', which is depicted in figure 23 (top). Between 50 Hz and 10 kHz, the $\varepsilon_r' \approx |\underline{\varepsilon}_r|$ of the material slightly decreases, meaning that toward higher frequencies, the electric field in the air gap between the upper electrode and the epoxy sample is weaker, thus requiring a higher test voltage to reach the same value as at lower frequencies. Consequently, the PDIV should be increased accordingly, as was shown, for instance, in [72]. Regarding the difference between the PDIVs measured at dry and high humidity conditions, one might note that the relative permittivity trend at high humidity (RH = 80%) of figure 23 is shifted evenly downward with respect to the trend observed under dry conditions. In line with the previous explanation, this shift should result in lower values of the PDIV for the high humidity conditions, which indeed corresponds to the experimental observations. A general decreasing tendency of the PDIV with increasing RH is often cited in literature, such as in [30]. Unfortunately, the behavior of the PDIV under PWM stresses could not be investigated due to limitations of the PD measurement equipment under these conditions.

4.2. PD aging

The aging results of non-coated samples show that below the PDIV, no significant aging seems to have occurred, as evidenced by the unchanged breakdown strength compared to non-aged samples. Conversely, all sample sets aged above the PDIV, have an evidently lower residual breakdown strength than the non-aged samples already after 0.5 h of aging. A slightly stronger degradation effect of the samples aged at higher peak voltage of one polarity ('9.9 kV(+)' and '9.9 kV(−)') compared to '7.5 kV(=)' might be present in figure 8 (however, the high scatter does not allow a more explicit statement).

By looking at the PRPD patterns shown in figure 7, it is clear that the PD activity is strongly affected by surface charge deposited on the epoxy sample (PDs occur even prior to the test voltage zero-crossings) caused by the discharges within the air gap between the spherical electrode and the sample surface. This implies that the peak-to-peak voltage rather than the maximum absolute peak voltage (related to the voltage zero) should determine the intensity of the PD activity and hence

presumably the degradation. In line with this assumption, no direct effect of a much larger absolute peak voltage on the degradation was observed in [20, 73]; however, the employed test voltage consisted of both DC and AC components and might thus not be directly applicable to our work (aging carried out under AC + PWM stresses). Other than that, two additional facts are indicated by the PD aging results: there seems to be no effect of the PWM pulses' polarity on the degradation ('9.9 kV(+)' vs. '9.9 kV(−)' in figure 8) and the samples appear to age faster under the high humidity conditions ('H' vs. 'D' breakdown strength data sets above the PDIV).

The latter claim seemingly conflicts with the PRPD patterns for dry and high-humidity conditions, which show that both the discharge magnitude and the average discharge current is larger for the dry conditions. Intuitively, stronger average discharges could be expected to lead to a faster degradation rate, but in case of epoxy, it has been shown that the degradation due to the kinetic energy of the ions formed during PDs is substantially weaker than the chemical degradation by reactive by-products also released during PDs [37]. This is supported by findings of [38], which show that a higher PD amplitude not necessarily leads to stronger aging. Furthermore, under high-humidity conditions, nitric, nitrous and oxalic acids are generated in addition to the by-products formed just in dry air. These acids were linked to the more severe degradation of epoxy due to PDs under high humidity conditions [36, 37], which aligns with the observations in the present work.

4.3. PD-free aging under hygroelectric stress

In the absence of humidity and elevated temperatures, the MF-MV aging regime applied to silver-coated samples (i.e., in the absence of PDs) was found to be without effect on all considered aging markers. At high RH levels, however, a dependence of aging on the RMS voltage stress at constant peak voltage stress was observed for all alternating voltage stresses (i.e. both AC + PWM and pure PWM voltages), but not for DC voltage stress (figure 17). In the opposite case, i.e. aging at constant RMS voltage stress, no influence of the peak voltage stress could be detected (figure 14). This is a remarkable finding as it points out that aging in the absence of both PDs and dielectric heating depends on the RMS voltage stress and not on the peak voltage stress, which contrasts with aging in the PD regime.

As the applied RMS voltage is related to the amount of electrical energy that is dissipated within the sample, it points out the presence of an aging mechanism related to the electrical energy input. A rather convincing explanation for the underlying mechanism can be found in the context of the electromechanical aging model proposed by Parpal *et al* [54], since this model not only describes an aging mechanism, which depends on the (e.g. electrical or thermal) energy input (as it is the case also for other models, e.g. [48, 49, 51]), but also gives a physical explanation which matches the findings of this work.

Within this model, the early onset of aging is attributed to a rearrangement of the free volume under electric field stress, which can take place in amorphous regions, which are obviously present in an amorphous polymer as the epoxy used

in this work. This might lead to a higher probability of a long free path, along which electrons can be accelerated over increasing distances under the influence of an electric field [74]. This effect is expected to be pronounced for higher RMS voltage stress values (thus matching the results of this work) by the higher energy input and the corresponding stronger deflection of the polymer chains, leading (locally) to larger free volume fractions. As a consequence, it is assumed that more high-energy electrons, which could subsequently break intermolecular van der Waals bonds [54], are present locally (not macroscopically), thus initiating stronger aging of the polymer. This idea of a localized material alteration could explain the findings of an earlier study [16] that of all investigated potential aging markers, only the breakdown strength, i.e. the only method that is sensitive to a very localized degradation (leading to a weak link for the initiation of a breakdown), could indicate aging effects. This hypothesis is further supported by the strong influence of humidity on the aging behavior as the potential energy barrier for the breaking of van der Waals bonds is found to be lowered by the presence of water [54].

Moreover, these findings support the hypothesis, made in an earlier work [16], of local (microscopic) morphological changes in the polymer structure occurring under MF-MV stress in the presence of (absorbed) water.

4.4. PD-free aging under thermoelectrical stress

Under the thermoelectrical stress profiles, the epoxy samples experienced aging effects similar to those under the hygroelectrical stress profiles. Note that the reduction in breakdown strength after electrical stress of $V_{RMS} = 4.43$ kV was found to be stronger at ambient temperature and RH $= 75\%$ (figure 10) compared to 70 °C and dry conditions (figure 12). However, a direct comparison between different thermoelectric and hygroelectric stress levels is not meaningful. The observed aging effects under thermoelectric stress might be attributable to the additional thermal energy input by the elevated temperature, which contributes to thermally activated electromechanical aging [54]. It should be mentioned that a potential contribution of dielectric heating could be excluded by experimentally validated thermoelectrical simulations shown in an earlier work [16].

4.5. Aging under non-electrical stress

Note that hydrolysis could be ruled out as a potential aging mechanism due to the absence of changes in the absorbance peak related to the hydroxyl group, as observed by FTIR measurements [16, 70]. A potential moisture-induced, irreversible plasticization, i.e. lowering of the glass transition temperature T_g, could as well be excluded by DSC measurements [16]. For pure humidity stress, pure temperature stress and even for hygrothermal stress below $T_g \approx 123$ °C, no aging effects were observed for the epoxy samples (figure 11). This again indicates the necessity of the presence of an alternating electric field stress, potentially favoring a (cyclic) movement of polymer

structures, for the onset of aging under the experimental conditions in this work.

However, one exception for aging in the absence of electrical stress was found, namely if aging was carried out above T_g. This coincides with changes of the optical appearance of the samples, more precisely a darker sample color, as well as with a significant thickness reduction. It is thus assumed that the reduced breakdown strength of the epoxy samples was caused by excessive post-curing, making them thinner, more brittle and thus potentially more prone to a dielectric breakdown.

4.6. PD-free aging under different electrical stress parameters

It should be noted that hygroelectrical stress profiles were used in order to systematically study further stress parameters (polarity of maximum voltage stress, type of MF-MV waveform, slew rate, PWM frequency, aging time) as they resulted in the strongest evidence of aging.

First of all, the influence of the polarity of the sinusoidal half-wave in which the maximum voltage stress occurred was found to be negligible, see figures 10 and 15. This can be explained by the almost symmetrical shape of the silver-coated recessed samples, which makes it less likely for a polarity effect to occur.

Space charge effects are assumed to be negligible, which is based on the finding that a DC offset voltage, which introduces space charges into the dielectric, had no measurable effect on aging under the experimental conditions used in this work (figure 17). It was indeed found that pure PWM stress led to the same aging effects as DC + PWM stress, even if the latter introduced a 3.4 times higher total RMS stress, but at the same PWM stress level. A comparison of the alternating voltage waveforms (pure AC, pure PWM and AC + PWM) in figure 16 reveals that MF voltage stress led to a stronger reduction in the breakdown strength than single-frequency voltage stress, indicating the presence and superposition of more than one aging mechanism for MF voltage waveforms.

The influence of the slew rate on aging below PD inception was found to be negligible for the values ($0.15\,\mathrm{kV}\,\mu s^{-1}$ and $38.9\,\mathrm{kV}\,\mu s^{-1}$) studied in this work (figure 18). Note that even if a higher slew rate itself does not lead to more severe aging, the voltage transition in some applications might be short enough to favor resonance effects and hence a voltage overshoot that might be higher than the PDIV. This, in turn, might lead to unexpected PD-related aging (while the RMS voltage is not significantly altered).

Variation of the PWM frequency revealed a remarkable effect on aging for both pure PWM as well as for AC + PWM voltage stress, namely a reduction in breakdown strength with *decreasing* PWM frequency (figures 19 and 20). A possible explanation for the observed PWM frequency dependence of the short-term AC breakdown strength can be given with the help of figure 23 in which the real part as well as the imaginary part of the complex relative permittivity of the investigated epoxy samples are displayed at $10\,^\circ\mathrm{C}$ and different RH levels. It is visible that the imaginary part increases towards

higher frequencies, i.e. a relaxation peak emerges (with the maximum at higher frequencies than measurable in this work). This means that the molecular side chains associated with this β relaxation [3, 75] transition from a state in which the chains can easily follow the alternating electric field changes to a state in which the steric hindrance of the side chain by other molecules is too high to follow the electric field changes of higher frequencies. As a consequence, the favored movement of side chains at lower frequencies will result in a stronger rearrangement of the free volume (according to the electromechanical aging model [54]) in the low-frequency range.

Moreover, the β relaxation is stronger and the absorbed water inside the sample is higher (visible by the steeper ε_r'' increase towards higher frequencies above $f_{AC} = 50\,\mathrm{Hz}$ for higher RH values in figure 23). Thus, the reduction in polymer chain movement according to the alternating electric field stress gets similarly stronger (and hence the suggested rearrangement of the free volume is less pronounced). Since the same β relaxation was not altered by MF-MV aging (shown in an earlier work [16]), it is confirmed that indeed not the molecular side chains themselves are altered under the employed stress conditions, which also supports the concept of the free volume rearrangement.

Note that at the highest investigated switching frequency $f_{PWM} = 40\,\mathrm{kHz}$, only minor aging effects were observed, despite the superimposed AC (50 Hz) voltage. This points out that of the two (or more) assumed aging mechanisms for both AC and PWM frequency components, the high-frequency component (in the kHz range) seems to be able to suppress/alter the aging influence of the low-frequency (50 Hz) component. This interesting finding needs more investigations in order to clearly identify the relevant molecular structures involved in the aging process.

As expected, longer aging times were found to lead to increasingly severe aging (figure 21). However, the onset of measurable aging effects (i.e. reduction in the breakdown strength) were observed after $0.5 \dots 5\,\mathrm{h}$. This means that the aged polymer structures exhibit aging effects not immediately, but after a specific period of time, which might be necessary for the hypothesized formation and/or growth of microcracks. The finding corresponds to earlier models for solid insulation aging, such as by [76, 77].

Another relevant finding is the fairly good correlation between the reduction in breakdown strength of the samples measured after different aging sequences and the number of sample failures that occurred before the intended end of aging under the same stress conditions, respectively. This is considered as a clear indication that the residual breakdown strength after aging is related to the lifetime of the insulation material. As a consequence, the findings obtained by residual breakdown strength measurements can be transferred to make statements about lifetime-influencing aging conditions.

Other material properties such as the real and imaginary part of the complex relative permittivity, the volume DC resistivity, the glass transition temperature as well as FTIR spectra were investigated in the context of this work (more detailed described in [16]). They consistently did not show

J. Phys. D: Appl. Phys. **56** (2023) 354005

F Küchler *et al*

any changes, even at the aging conditions with the most severe breakdown strength reduction. However, all of these potential aging markers focus on integral macroscopic material properties, whereas the breakdown strength can be also influenced by—and is often determined by—local microscopical changes that might lead to the initiation of a dielectric breakdown path. These observations are thus in accordance with the earlier mentioned hypothesis of electromechanically induced morphological material changes on a microscopical scale, more precisely a rearrangement of the free volume in amorphous regions, which favors the breaking of van der Waals bonds.

Moreover, the results of this work underline the conclusion drawn in [16] that the absence of any aging-induced changes for all of the investigated aging markers except for the AC breakdown strength represent a clear issue for aging evaluation of polymeric insulation materials. This is due to the fact that relevant aging (shown by a reduction of the residual breakdown strength) is not observable by a broad range of non-destructive aging markers and thus, aging effects might be underestimated in real applications (when quantified by these non-destructive aging markers, such as permittivity, loss factor or resistivity measurements).

The findings in this work indicate that even if the comparatively strong risk factors for insulation aging, namely PD activity and dielectric heating, can be excluded, aging effects under MF-MV stress profiles still exist. However, if high humidity levels and high temperatures can be avoided (which might not always be possible), power electronic devices are expected to be operated much more reliably.

5. Conclusion and outlook

In the present contribution, the influence of MF-MV and environmental stress on the aging behavior of epoxy samples was studied over a broad range of parameter variations. The key findings are summarized in the following:

- PD-related aging due to material erosion is dependent on the peak-to-peak voltage stress (in accordance with available literature) and occurs on a significantly shorter timescale than PD-free aging, especially at high RH levels.
- Pure electrical MF-MV stress at dry conditions has no influence on aging under the studied conditions if in the absence of PDs and dielectric heating.
- Non-electrical stress is critical only above a certain temperature, most likely the glass transition temperature.
- PD-free aging is independent of the peak voltage stress (in case of constant RMS voltage stress and frequency).
- PD-free aging in the presence of water (and/or most likely at elevated temperatures) is dependent on the RMS voltage stress, which is related to the energy input.
- Aging dependence on the RMS voltage stress is only present for alternating voltage components, but not for DC voltage components.
- Space charge effects on aging are rather unlikely as no effect of a DC voltage offset is observed.

- Aging below PDIV under the conditions in this work is not influenced by different slew rates.
- Less aging takes places at higher PWM frequencies, which might be attributed to the steric hindrance of polymer side chains moved by the alternating electric field.
- MF voltages exhibit superimposed aging mechanisms attributed to the respective single-frequency components.
- Aging onset does not happen immediately, but only after a specific period of time.
- The residual AC breakdown strength correlates with insulation lifetime observations for the used epoxy samples in the absence of PDs.
- Relevant insulation aging (indicated by a reduction in AC breakdown strength) is not observable by a broad range of non-destructive aging markers.
- The hypothesis of the electromechanically induced rearrangement of the free volume, followed by the local breaking of van der Waals bonds by high-energy electrons as a dominant aging mechanism in the absence of PDs, is supported by the measurement results in this work.

In a next step, it is recommended to investigate the aforementioned hypothesis of free volume rearrangement with subsequent breaking of van der Waals bonds in detail. For this purpose, other diagnostics, e.g. microscopic tools or methods suggested by [54], such as small-angle x-ray scattering, small-angle neutron scattering or positron annihilation will be needed in order to detect such small morphological material changes. However, as the changes relevant for critical aging are hypothesized to occur only very localized, the experimental detection is expected to be challenging. Nevertheless, the obtained results of this work can already be used to optimize the insulation material for applications which are exposed to MF-MV and environmental stress. Promising results are expected if it is possible to modify the material in a way that its performance in the presence of water and elevated temperatures is enhanced, e.g. by reducing the material's tendency to absorb water or increasing its glass transition temperature. Furthermore, it is recommended to test the generality of the findings for other types of polymers, e.g. for semicrystalline materials, having a lower amount of amorphous areas (in which free volume can exist).

Data availability statement

The data that supports the findings of this study are available upon reasonable request from the authors.

Acknowledgments

ORCID iDs

Florian Küchler 🔘 https://orcid.org/0000-0002-1526-3888
Christian M Franck 🔘 https://orcid.org/0000-0002-2201-7327

References

[1] Hannan M A, Lipu M S L, Ker P J, Begum R A, Agelidis V G and Blaabjerg F 2019 Power electronics contribution to renewable energy conversion addressing emission reduction: applications, issues and recommendations *Appl. Energy* **251** 1–25

[2] Huang A Q, Crow M L, Heydt G T, Zheng J P and Dale S J 2011 The future renewable electric energy delivery and management (FREEDM) system: the energy Internet *Proc. IEEE* **99** 133–48

[3] Li J, Guo P, Kong X, Wang Y, Li F and Du B 2022 Curing degree dependence of dielectric properties of bisphenol-A-based epoxy resin cured with methyl hexahydrophthalic anhydride *IEEE Trans. Dielectr. Electr. Insul.* **29** 2072–9

[4] Kolar J W and Ortiz G 2014 Solid-state-transformers: key components of future traction and smart grid systems *Proc. IEEE Int. Power Electronics Conf.* vol 7

[5] Madonna V, Giangrande P and Galea M 2018 Electrical power generation in aircraft: review, challenges and opportunities *IEEE Trans. Transp. Electrif.* **4** 646–59

[6] Rosero J, Ortega J, Aldabas E and Romeral L 2007 Moving towards a more electric aircraft *IEEE Aerosp. Electron. Syst. Mag.* **22** 3–9

[7] Ji S, Zheng S, Wang F and Tolbert L M 2018 Temperature-dependent characterization, modeling and switching speed limitation analysis of third generation 10 kV SiC MOSFET *IEEE Trans. Power Electron.* **33** 4317–27

[8] Oswald N, Anthony P, McNeill N and Stark B H 2014 An experimental investigation of the tradeoff between switching losses and EMI generation with hard-switched All-Si, Si-SiC and All-SiC device combinations *IEEE Trans. Power Electron.* **29** 2393–407

[9] Wang Y, Lucia O, Zhang Z, Gao S, Guan Y and Xu D 2020 A review of high frequency power converters and related technologies *IEEE Open J. Indust. Electron. Soc.* **1** 247–60

[10] Okumura H 2015 A roadmap for future wide bandgap semiconductor power electronics *MRS Bull.* **40** 439–44

[11] Östling M, Ghandi R and Zetterling C-M 2011 SiC power devices—present status, applications and future perspective *IEEE Proc. Int. Symp. Power Semiconductor Devices & IC's* vol 23 pp 10–15

[12] Dimitrijev S, Han J, Moghadam H A and Aminbeidokhti A 2015 Power-switching applications beyond silicon: status and future prospects of SiC and GaN devices *MRS Bull.* **40** 399–405

[13] Cleland J G, McCormick V E and Turner M W 1995 Design of an efficiency optimization controller for inverter-fed AC induction motors *IEEE Conf. Record Industry Applications Conf.* vol 30 pp 16–21

[14] Jung C 2017 Power up with 800-V Systems: the benefits of upgrading voltage power for battery-electric passenger vehicles *IEEE Electrif. Mag.* **5** 53–58

[15] Aghabali I, Bauman J, Kollmeyer P J, Wang Y, Bilgin B and Emadi A 2021 800-V electric vehicle powertrains: review and analysis of benefits, challenges and future trends *IEEE Trans. Transp. Electrif.* **7** 927–48

[16] Küchler F, Färber R, Bill F, Renggli S and Franck C M 2023 Mixed-frequency medium-voltage aging analysis of epoxy in the absence of partial discharges and dielectric heating *J. Phys. D: Appl. Phys.* accepted (https://doi.org/10.1088/1361-6463/acd85a)

[17] Stone G C and Culbert I 2014 Review of stator insulation problems in medium voltage motors fed from voltage source PWM drives *Proc. Int. Symp. Electrical Insulating Materials* pp 50–53

[18] Haq S U, Jayaram S H, Cherney E A and Simon L C 2006 Partial discharge erosion of nano-filled enameled wires subjected to high frequency waveforms *Conf. Record Int. Symp. Electrical Insulation* pp 396–9

[19] Kaufhold M, Börner G, Eberhardt M and Speck J 1996 Failure mechanism of the interturn insulation of low voltage electric machines fed by pulse-controlled inverters *IEEE Electr. Insul. Mag.* **12** 9–16

[20] Färber R, Guillod T, Krismer F, Kolar J W and Franck C M 2020 Endurance of polymeric insulation foil exposed to DC-biased medium-frequency rectangular pulse voltage stress *Energies* **13** 13

[21] Wang P, Cavallini A, Montanari G C and Wu G 2013 Effect of rise time on PD pulse features under repetitive square wave voltages *IEEE Trans. Dielectr. Electr. Insul.* **20** 245–54

[22] Pauli F, Ruf A and Hameyer K 2020 Low voltage winding insulation systems under the influence of high du/dt slew rate inverter voltage *Arch. Electr. Eng.* **69** 187–202

[23] Yin W 1997 Failure mechanism of winding insulations in inverter-fed motors *IEEE Electr. Insul. Mag.* **13** 18–23

[24] Stranges M K W, Stone G C and Bogh D L 2009 Voltage endurance testing—stator insulation systems for inverter-fed machines *IEEE Ind. Appl. Mag.* **15** 12–18

[25] Hammarström T J, Bengtsson T, Blennow J and Gubanski S M 2014 Partial discharges in motor wires at PWM voltages of different smoothness *Proc. Int. Symp. on Electrical Insulating Materials* pp 184–7

[26] Bengtsson T, Dijkhuizen F, Ming L, Sahlen F, Liljestrand L, Bormann D, Papazyan R and Dahlgren M 2009 Repetitive fast voltage stresses-causes and effects *IEEE Electr. Insul. Mag.* **25** 26–39

[27] Lusuardi L and Cavallini A 2018 The problem of altitude when qualifying the insulating system of actuators for more electrical aircraft *Proc. IEEE Int. Conf. on Electrical Systems for Aircraft, Railway, Ship Propulsion and Road Vehicles & Int. Transportation Electrification Conf.* pp 1–4

[28] Kandev N, Castelan P, Lebey T, Amyot N and Hudon C 2000 Testing of low-voltage motor turn insulation intended for pulse-width modulated applications *IEEE Trans. Dielectr. Electr. Insul.* **7** 783–9

[29] Binder E, Draxler A, Muhr M, Pack S, Schwarz S, Egger H and Hummer A 1999 Effects of air humidity and temperature to the activities of external partial discharges of stator windings *Proc. Int. Symp. on High Voltage Engineering* pp 264–7

[30] Fenger M and Stone G C 2005 Investigations into the effect of humidity on stator winding partial discharges *IEEE Trans. Dielectr. Electr. Insul.* **12** 341–6

[31] Soltani R, David E and Lamarre L 2009 Study on the effect of humidity on dielectric response and partial discharges activity of machine insulation materials *IEEE Electrical Insulation Conf.* pp 343–7

[32] Guastavino F and Tiemblo P 1998 Effect of humidity on the time to breakdown of polymers subject to partial discharges *Polym. Eng. Sci.* **38** 119–26

[33] Guastavino F and Ratto A 2012 Comparison between conventional and nanofilled enamels under different environmental conditions *IEEE Electr. Insul. Mag.* **28** 35–41

[34] Ehara Y, Aono K and Koshio S 2016 Degradation analysis of epoxy resin surfaces exposed to partial discharge *IEEE Conf. on Electrical Insulation and Dielectric Phenomena* pp 881–4

[35] Küchler F, Färber R and Franck C M 2020 Effect of humidity on lifetime and dielectric properties of PET film *IEEE Int. Conf. Dielectrics* vol 3 pp 101–5

[36] Shields A J, Cooper I J, Kemp I J and Hepburn D M 2000 Degradation of epoxy resin by partial discharges *IEE Proc.-Sci. Meas. Technol* **147** 97–104

[37] Müller N, Lang S and Moos R 2019 Influence of ambient conditions on electrical partial discharge resistance of epoxy anhydride based polymers using IEC 60343 method *IEEE Trans. Dielectr. Electr. Insul.* **26** 1463–70

[38] Guastavino F, Dardano A, Ratto A and Torello E 2009 Electrical aging test on twisted pair specimens under different environmental conditions *IEEE Conf. on Electrical Insulation and Dielectric Phenomena* pp 81–84

[39] Sonerud B, Bengtsson T, Blennow J and Gubanski S M 2009 Dielectric heating in insulating materials subjected to voltage waveforms with high harmonic content *IEEE Trans. Dielectr. Electr. Insul.* **16** 926–33

[40] Birle M and Leu C 2013 Dielectric heating in insulating materials at high DC and AC voltages superimposed by high frequency high voltages *Proc. Int. Symp. High Voltage Engineering* vol 18 pp 1025–30

[41] König D, Hardt N and Scherb V 1998 Comparitive insulation tests with DC and AC at 50 Hz and 50 kHz *Report Conf. Electrical Insulation and Dielectric Phenomena* vol 2 pp 702–5

[42] Guillod T, Färber R, Rothmund D, Krismer F, Franck C M and Kolar J W 2020 Dielectric losses in dry-type insulation of medium-voltage power electronic converters *IEEE J. Emerg. Sel. Top. Power Electron.* **8** 2716–32

[43] Birle M and Leu C 2013 Breakdown of polymer dielectrics at high direct and alternating voltages superimposed by high frequency high voltages *IEEE Int. Conf. Solid Dielectrics* pp 656–61

[44] Niayesh K and Gockenbach E 2014 On the aging mechanism of solid insulating materials exposed to repetitive high voltage pulses *IEEE Trans. Dielectr. Electr. Insul.* **21** 304–10

[45] Fabiani D, Montanari G C and Contin A 2001 Aging acceleration of insulating materials for electrical machine windings supplied by PWM in the presence and in the absence of partial discharges *IEEE Int. Conf. Solid Dielectrics* vol 7 pp 283–6

[46] Stone G C, van Heeswijk R G and Bartnikas R 1992 Investigation of the effect of repetitive voltage surges on epoxy insulation *IEEE Trans. Energy Convers.* **7** 754–60

[47] Gao B, Wu G N, He J Y and Lei K G 2007 Investigation on aging mechanism of winding insulation used in inverter-fed traction motors *Report Conf. Electrical Insulation and Dielectric Phenomena* pp 107–11

[48] Zeller H R and Schneider W R 1984 Electrofracture mechanics of dielectric aging *J. Phys. D: Appl. Phys.* **56** 455–9

[49] Dissado L A, Mazzanti G and Montanari G C 1997 The role of trapped space charges in the electrical aging of insulating materials *IEEE Trans. Dielectr. Electr. Insul.* **4** 496–506

[50] Crine J-P, Parpal J-L and Lessard G 1989 A model of aging of dielectric extruded cables *Proc. Int. Conf. Conduction and Breakdown in Solid Dielectrics* pp 347–51

[51] Jones J P, Llewellyn J P and Lewis T J 2005 The contribution of field-induced morphological change to the electrical aging and breakdown of polyethylene *IEEE Trans. Dielectr. Electr. Insul.* **12** 951–66

[52] Griffith A A 1921 The phenomena of rupture and flow in solids *Phil. Trans. R. Soc.* **221** 163–98

[53] Lustiger A and Markham R L 1983 Importance of tie molecules in preventing polyethylene fracture under long-term loading conditions *Polymer* **24** 1647–54

[54] Parpal J-L, Crine J-P and Dang C 1997 Electrical aging of extruded dielectric cables—a physical model *IEEE Trans. Dielectr. Electr. Insul.* **4** 197–209

[55] Blythe A R and Bloor D 2005 *Electrical Properties of Polymers* vol 2 (Cambridge: Cambridge University Press)

[56] Sanche L 1997 Nanoscopic aspects of electronic aging in dielectrics *IEEE Trans. Dielectr. Electr. Insul.* **4** 507–43

[57] Crine J-P 1998 Electrical, chemical and mechanical processes in water treeing *IEEE Trans. Dielectr. Electr. Insul.* **5** 681–94

[58] Bascom W D 1970 Water at the Interface *J. Adhes.* **2** 161–83

[59] Meyer C T and Filippini J C 1979 Water-treeing seen as an environmental stress cracking phenomenon of electric origin *Polymer* **20** 1186–7

[60] Crine J-P and Jow J 2001 Influence of frequency on water tree growth in various test cells *IEEE Trans. Dielectr. Electr. Insul.* **8** 1082–7

[61] ISO 62:2008 2008 *Plastics—Determination of Water Absorption* vol 3 (International Standard)

[62] Küchler F, Färber R and Franck C M 2020 Humidity and temperature effects on the dielectric properties of PET film *IEEE Electrical Insulation Conf.* pp 179–83

[63] IEC 60270:2000+A1:2015 2015 *High-Voltage Test Techniques—Partial Discharge Measurements* vol 3 (International Standard)

[64] IEC TS 61934:2011 2011 *Electrical Insulating Materials and Systems—Electrical Measurement of Partial Discharges (PD) Under Short Rise Time and Repetitive Voltage Impulses* vol 2 (International Standard)

[65] Šefl O, Färber R and Franck C M 2023 On the frequency dependence of the PDIV in twisted pair magnet wire analogy in dry air *IEEE Trans. Dielectr. Electr. Insul.* submitted

[66] IEC 60243-1:2013 2013 *Electrical Strength of Insulating Materials—Test Methods—Part 1: Test at Power Frequencies* vol 3 (International Standard)

[67] ASTM D149-09 2013 *Standard Test Method for Dielectric Breakdown Voltage and Dielectric Strength of Solid Electrical Insulating Materials at Commercial Power Frequencies* (American National Standard)

[68] Färber R and Franck C M 2018 Modular high-precision dielectric spectrometer for quantifying the aging dynamics in (Sub-)picofarad polymeric specimens *IEEE Trans. Dielectr. Electr. Insul.* **25** 1056–63

[69] Küchler F, Lötscher E R, Färber R and Franck C M 2021 Polarization-depolarization current (PDC) measurements for volume and surface resistivity analysis of polymeric materials *IEEE Conf. on Electrical Insulation and Dielectric Phenomena* pp 17–22

[70] Andersson J, Gubanski S M and Hillborg H 2008 Properties of interfaces between silicone rubber and epoxy *IEEE Trans. Dielectr. Electr. Insul.* **15** 1360–7

[71] Electrolube 2014 *Silver Conductive Paint (Technical Data Sheet)*

[72] Wada K, Tsuji K and Muto H 2003 Partial discharge inception voltage for two insulating materials (PVC and PE) under inverter surge voltage *Proc. Int. Conf. Properties and Applications of Dielectric Materials* pp 847–50

[73] Linde T, Backhaus K, Schlegel S, Lengsfeld S and Steffen J 2022 Partial discharge behavior of epoxy-mica insulation system under superimposed AC and DC voltage stress *Proc. Nordic Insulation Symp.* vol 27 pp 1–6

J. Phys. D: Appl. Phys. **56** (2023) 354005

F Küchler *et al*

[74] Artbauer J 1996 Electric strength of polymers *J. Phys. D: Appl. Phys.* **29** 446–56

[75] Saeedi I A, Andritsch T and Vaughan A S 2019 On the dielectric behavior of amine and anhydride cured epoxy resins modified using multi-terminal epoxy functional network modifier *Polymers* **11** 1–18

[76] Kako Y, Kadotani K and Tsukui T 1983 An analysis of combined stress degradation of coil insulation in case of semi-log V-t expression *IEEJ Trans. Fundam. Mater.* **103** 53–60

[77] Kahle M 1988 *Elektrische Isoliertechnik* vol 1 (Berlin: VEB Verlag Technik) p 211